# Reduced Damage From Facing-Target Sputtering of Indium Tin Oxide Films

by

Gillian L. Hagen

Submitted to the Department of Physics
in partial fulfillment of the requirements for the degree of

Bachelors of Arts

at

Mount Holyoke College

May 2020

©Mount Holyoke College

Author .....
Department of Physics
May 3, 2020

Certified by .....
Alexi C. Arango
Assistant Professor of Physics
Thesis Supervisor

Accepted by .....
Alexi C. Arango
Chair, Department of Physics

# Reduced Damage From Facing-Target Sputtering of Indium Tin Oxide Films

by

Gillian L. Hagen

Submitted to the Department of Physics
on May 3, 2020, in partial fulfillment of the
requirements for the degree of
Bachelors of Arts

## Abstract

This study addresses a current limitation in the development of high performance organic optoelectronic devices: depositing indium tin oxide (ITO), a transparent, conductive film, without damage to underlying organic films. ITO is deposited with a plasma sputter deposition process which causes damage to organic films. Previous research demonstrates that damage can be reduced with a sputtering configuration with substrates placed perpendicular to two facing guns. We employ fluorescent organic material $Alq_3$ (tris-(8-hydroxyquinoline)aluminum) to explore damage caused by radio-frequency facing-target magnetron plasma sputtering by means of photoluminescence spectroscopy. We present an investigation of the degree to which $Alq_3$ is damaged in the plasma sputtering process. We explore the dependence of the damage on the rate of growth. We evaluate the effects of closing the sputter system shutter to eliminate direct plasma exposure as well as the effect of employing a BPhen (bathophenanthroline) protective layer. We find that facing-target sputtering can be performed at a high growth rate without causing significantly more damage than that caused when sputtering is performed at a low growth rate, with only a 10% reduction in PL from a rate of 0.2Å/s to 2.4Å/s. We demonstrate that the greatest amount of damage occurs at the start of plasma sputtering. The BPhen protective layer is shown to mitigate damage to the surface of the organic material by exposure to gaseous ions.

Thesis Supervisor: Alexi C. Arango
Title: Assistant Professor of Physics

# Acknowledgments

Thank you to Professor Alexi Arango, who has served as both my research and academic advisor at Mount Holyoke. Professor Arango's Electromagnetism course provided my start in Physics and introduction to the Mount Holyoke Physics community. Thank you for introducing me to scientific research and for providing me the opportunity to pursue research following my first year with a Lynk UAF program grant. My path would likely be very different without such opportunities.

Thank you to the entire Mount Holyoke Physics Department, including Professor Kathy Aidala, Professor Spencer Smith, Professor Kerstin Nordstrom, Professor Mark Peterson, and Visiting Professor Anat Burger. Thank you to Sarah Byrne and Nicole Amrani who provided support as Department Coordinators throughout my time at Mount Holyoke.

Thank you to Professor Maria Gomez and Professor Mark Peterson for their engaging instruction and for serving on my thesis committee.

Thank you to my summer research advisors: Professor Sossina Haile at Northwestern University and Dr. Andrew Ferguson at the National Renewable Energy Laboratory.

Thank you to past and present members of the Arango Lab, including Sophia Weeks, Kathleen Smith, Sue Shi, Jessie Guo, Maryann Valerio, Anne Bevin, Ji-Won Ham, and Hadley O'Malia. Thank you to Dr. Christina McGahan who has been a great friend and mentor over the years.

I am grateful for the opportunity to receive a Mount Holyoke education through support of the following scholarships: Mount Holyoke 21st Century Scholarship; 2020 Fleur Varney Chandler, Class of 1955, Endowed Scholarship; 2019 Fleur Varney Chandler, Class of 1955, Endowed Scholarship; 2018 Mary Bishop Whitney, Class of 1859, Endowed Scholarship; National Honor Society Chapter Scholarship; Highland High School PTO Scholarship Award; Highland High School Education Association Scholarship Award; Hugh and Grace Eyerdom Memorial Scholarship; Highland Foundation Scholarship for Educational Excellence.

I would like to acknowledge that Mount Holyoke College sits on Nonotuck land. I would also like to acknowledge neighboring Indigenous nations: the Nipmuc and the Wampanoag to the East, the Mohegan and Pequot to the South, the Mohican to the West, and the Abenaki to the North.

Thank you to my Mount Holyoke friends. It has been a privilege to be surrounded by people with such passion and determination.

I express my gratitude to the O'Malia family, Matthew, Heather, Hadley, Finnian, and Liam, who generously hosted me during the COVID-19 pandemic while I finished this work.

Thank you to Alyson Hagen, Hannah Stein, Kenneth Crossley, Nathan Agarwal, and Tamara Koledin for the adventures, humor, and friendship.

Thank you to Deputy Sharon Centner, Mrs. Tanya Dolata, Mrs. Claudia Johnson, Mrs. Kristine Chirici, and Mr. Rob Schmelzer for providing support and believing in my potential before I did.

Thank you to my entire family.

# Contents


**1 Introduction** **13**

1.1 Transparent Conductive Electrodes . . . . . 13

1.1.1 Indium Tin Oxide (ITO) and Other Transparent Conductive Materials . . . . . 13

1.2 Previous Research . . . . . 15

1.3 Investigation of Facing-Target Sputtering . . . . . 16

1.3.1 Research Questions . . . . . 16

1.3.2 Experimental Approach . . . . . 17

1.4 Summary . . . . . 19

**2 Theory** **21**

2.1 Plasma Sputter Deposition . . . . . 21

2.2 Damage Mechanisms . . . . . 24

2.3 Photoluminescence . . . . . 25

**3 Methods** **27**

3.1 Fabrication . . . . . 27

3.2 Plasma Sputter Deposition Trends . . . . . 28

3.3 Sample and Control Structures . . . . . 29

3.4 Photoluminescence Analysis Techniques . . . . . 31

**4 Results** **35**

4.1 Effect of ITO Film Deposition on Organic Film Damage . . . . . 35

4.1.1 Effect of Depositing ITO on a Fluorescent Organic Layer . . . 35
4.1.2 Effect of Depositing ITO on a Fluorescent Organic Layer with Protective Buffer Layer . . . 40
4.1.3 Consistent Organic Damage . . . 45
4.2 Plasma Sputter Shutter State . . . 49
4.3 Effect of Gaseous Ion Exposure . . . 49
4.4 Summary of Results . . . 54

**5 Discussion** **55**
5.1 Facing-Target Sputtering System . . . 55
5.2 Growth Rate . . . 55
5.3 Distinguishing Damage Mechanisms from PL . . . 57
5.3.1 Shutter State . . . 57
5.3.2 Plasma Sputtering Stages . . . 59
5.3.3 Damage by Plasma Sputter Stage . . . 59
5.4 Error and Control Measures . . . 60
5.5 Summary . . . 60

**6 Conclusion** **61**
6.1 Future work . . . 61
6.2 Impacts . . . 62

**A Appendix** **63**
A.1 Fluorescence . . . 63
A.2 Photoluminescence (PL) Analysis and Error Propagation Calculations 63
A.2.1 Addition of Measured PL . . . 63
A.2.2 Average PL . . . 63
A.2.3 Normalized PL . . . 64

# List of Figures


1-1 Molecular structure of ITO (Indium tin oxide) . . . . . 14

1-2 Molecular structure of (A) $Alq_3$ (tris(8-hydroxyquinolinato)aluminium) and (B) BPhen (Bathophenanthroline) . . . . . 17

1-3 Sputter System Shutter State . . . . . 18

2-1 Illustration of facing-target magnetron sputter system, where S and N indicate south and north magnetic poles. . . . . 22

2-2 Illustration of magnets in gun, from the perspective of the sputter system gun. . . . . 22

2-3 Sputter Shutter Open: Gaseous ions, high energy ions and electrons, and secondary electrons can bombard substrates. . . . . 23

2-4 Fluorescence: Electrons are represented by their spin state in blue arrows. High energy photons excite an electron from the ground state to an excited state. The electron relaxes to a lower energy state through thermal relaxation. Eventually, as the system reaches equilibrium, the electron relaxes to the ground state and emits a photon of lower energy. 26

3-1 Linear Trend Between Growth Rate and Growth Power . . . . . 28

3-2 Photoluminescence Spectroscopy Setup . . . . . 32

3-3 PL: Sample and Control Measurements . . . . . 33

4-1 Structure: glass / 40nm $Alq_3$ . . . . . 36

4-2 Structure: glass / 40nm $Alq_3$ / 10nm ITO . . . . . 36

4-3 ITO Film Without BPhen Protective Layer . . . . . 38

4-4 PL Spectra: glass / 40nm $Alq_3$ / 100nm ITO . . . . . 39
4-5 Structure: glass / 40nm $Alq_3$ / 7nm BPhen . . . . . 40
4-6 Structure: glass / 40nm $Alq_3$ / 7nm BPhen / 10nm ITO . . . . . 41
4-7 ITO Film Deposition With BPhen Protective Layer . . . . . 43
4-8 PL Spectra: glass / 40nm $Alq_3$ / 7nm BPhen / 100nm ITO . . . . . 44
4-9 ITO Deposition: Growth Rate vs. PL Ratio Comparison . . . . . 45
4-10 ITO Deposition: PL Spectra Comparison . . . . . 46
4-11 ITO Deposition: Illustrating Damage Rate vs. ITO Growth Rate . . 47
4-12 ITO Deposition: Illustrating Damage Rate vs. Growth Time . . . . . 48
4-13 Structure: glass / 40nm $Alq_3$ . . . . . 50
4-14 Structure: glass / 40nm $Alq_3$ / 7nm BPhen . . . . . 50
4-15 Gaseous Ion Exposure With and Without BPhen Protective Layer . . 51
4-16 PL Spectra: Gaseous Ion Exposure Without BPhen Protective Layer 52
4-17 PL Spectra: Gaseous Ion Exposure With BPhen Protective Layer . . 53

5-1 Sputter Shutter Open: ITO atoms, high energy ions and electrons, secondary electrons, and gaseous ions can bombard substrates. . . . . 58
5-2 Sputter Shutter Closed: High energy ions, electrons, and secondary electrons are confined to plasma plume, ITO atoms are shielded by the shutter, and gaseous ions are located throughout chamber. . . . . 58

# List of Tables


1.1 Field of Transparent Conductive Materials Adapted from Ellmer [1] . 14

3.1 ITO Deposition Sample Structures Without BPhen . . . . . 29
3.2 ITO Deposition Control Structures Without BPhen . . . . . 29
3.3 ITO Deposition Sample Structures With BPhen . . . . . 30
3.4 ITO Deposition Control Structures With BPhen . . . . . 30
3.5 Gaseous Ion Exposure Sample and Control Structures Without BPhen 31
3.6 Gaseous Ion Exposure Sample and Control Structures With BPhen . 31

4.1 ITO Deposition Sample Structures . . . . . 37
4.2 ITO Deposition Sample Structures With BPhen . . . . . 42

# Chapter 1

# Introduction

## 1.1 Transparent Conductive Electrodes

Transparent conductive electrodes (TCEs) are a key component of solar cells, light emitting diodes (LEDs), smart phones and televisions. [1, 2]. TCEs conduct electrical current while allowing light to enter and exit the device. [3]

### 1.1.1 Indium Tin Oxide (ITO) and Other Transparent Conductive Materials

Indium tin oxide (ITO) is the most widely used transparent conductive electrode material in organic light emitting diodes (OLEDs) and organic photovoltaics. The prominence of ITO can be attributed to its environmental stability and superior optoelectronic properties. [3] The molecular structure of ITO is illustrated in Figure 1-1.

Table 1.1, adapted from Ellmer [1], shows TCEs divided by material class. Current TCE materials being explored include metals, such as silver nanowires [4], semiconductor oxides, including ITO, as well as a recently emerged category of carbon TCEs, including carbon nanotube films and polymer composites. [5, 6, 7, 8]

Haacke's figure of merit, expressed in Equation 1.1, allows TCEs to be judged for

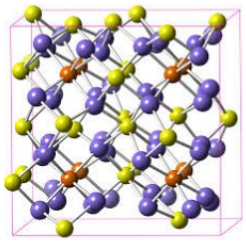


Figure 1-1: Molecular structure of ITO (Indium tin oxide)

their suitability in a particular application.

$$\Phi_H = \frac{T^q}{R_s} = \frac{T^q}{\alpha q} \tag{1.1}$$

The figure of merit accounts for the material properties of the potential TCE, where $T$ is transmittance, $R_s$ is sheet resistance, $q$ is an exponent which determines the transmittance necessary for a particular use, and $\alpha$ is the absorption coefficient.

Table 1.1: Field of Transparent Conductive Materials Adapted from Ellmer [1]

| **Material Class** | **Material** |
|---|---|
| Metals | Al |
| | Ag |
| | Cu |
| Semiconductors | ITO |
| | $SnO_2$ |
| | ZnO |
| | $TiO_2$ |
| | Si |
| Carbon | Polymers |
| | Single Walled Carbon Nanotubes |
| | Graphene |

ITO dominates over other TCEs in terms of its use in optoelectronic devices due to its superior properties. ITO holds highest figure of merit for TCEs.[1] Additionally, ITO has the lowest resistivity of all semiconductor TCEs produced on a commercial

scale, at approximately 1-2$\times 10^{-4}\Omega$ cm. [9] For this reason, ITO is the TCE material most commonly used in organic optoelectronics.

## 1.2 Previous Research

Transparent conductive electrodes (TCEs) are commonly employed as a bottom electrode in organic optoelectronic devices. The deposition of ITO as a top electrode opens up many new device possibilities, but remains a major fabrication challenge. ITO is typically deposited through plasma sputtering, a method which causes significant damage to organic layers, detailed in Chapter 2. As a consequence, a low growth rate is commonly used to reduce sputtering damage, extending the time required for deposition. [10, 11, 12] This fabrication limitation is a pressing issue which inhibits the realization of high performance organic optoelectronic devices.

Previous work has examined plasma sputtering damage caused to fluorescent organic material $Alq_3$ (tris(8-hydroxyquinolinato)aluminium) by means of photoluminescence spectroscopy, [13, 14, 15, 16, 11, 17, 18] whereby a decrease in photoluminescence correlates to organic film damage, detailed in 2. A 2010 study by Lei et al. examined the effect of plasma exposure to organic films through studying ion-induced damage to BAlq (Bis(8-hydroxy-2-methylquinoline)-(4-phenylphenoxy)aluminum) by measuring photoluminescence. They observed a decrease in Photoluminescence (PL) intensity upon electron bombardment. [17]

Past work has simulated the effect of ions generated during plasma sputtering to study organic layer damage. Liao et al. investigated the mechanism responsible for damage caused to $Alq_3$ films in OLEDs by simulating plasma with an Argon ion beam. They report broken chemical bonds at the $Alq_3$ surface using ultraviolet photoelectron spectroscopy and x-ray photoelectron spectroscopy. The study concludes that organic surface damage from sputtering significantly degrades OLED device performance when exposed high energy ions and no buffer layer is in place. [12]

As recommended by Liao et al., researchers have explored the use of oxide and metal buffer layers to reduce plasma sputtering damage induced to organic layers.

In 2013, Zhao et al. utilized BPhen (Bathophenanthroline) in polymer solar cells to eliminate exciton quenching at the electrode interface and protect the organic layer from damage caused by depositing a silver top electrode. [19, 20, 21]

While studies have investigated plasma sputtering damage caused to an organic fluorescent material by means of photoluminescence, no study has examined the fundamental mechanisms responsible for damage caused to an $Alq_3$ film when plasma sputtering ITO with a facing-target magnetron sputter system. Additionally, no previous study has investigated the use of BPhen as a protective layer in a fundamental study of organic film damage. [22]

## 1.3 Investigation of Facing-Target Sputtering

This study examines plasma sputtering performed with a unique radio-frequency facing-target magnetron sputter deposition system designed to minimize plasma induced damage. [23] In this design, substrates are placed above the plasma and a magnetic field is used to protect substrates from high energy ions and electrons. The details of the sputter system are explained in Chapter 2.

A 2013 study by Lei et al. shows that facing-target sputtering systems are better at reducing bombardment from negatively-charged oxygen ions and secondary electrons emitted from the charged sputtering target electrode compared to conventional magnetron sputtering, low voltage sputtering, and kinetic-energy-control-deposition systems. [24] Onai et al. specifically reported reduced damage from plasma sputtering ITO electrodes through use of facing-target sputtering. Their results were obtained through measuring the photoluminescence of BAlq samples bombarded with Argon ions and samples deposited with an ITO film. [25] This thesis presents a detailed analysis of the mechanism responsible for organic layer damage upon the plasma sputter deposition of ITO.

### 1.3.1 Research Questions

The main research questions include:

- What is the effect of ITO growth rate on plasma sputtering damage induced to organic layers?
- What is the role of a protective layer inserted between an organic layer and ITO electrode?
- What is the mechanism of plasma sputtering damage within radio-frequency facing-target magnetron plasma sputtering?

### 1.3.2 Experimental Approach

**Create material system for sputtering experiments:** We fabricate simple structures, detailed in Chapters 3 and 4, comprised of organic fluorescent material, $Alq_3$ (tris(8-hydroxyquinolinato)aluminium), illustrated in Figure 1-2, to be exposed to ITO (indium tin oxide) plasma sputtering.

**Assess sputtering induced damage using photoluminescence spectroscopy:** We analyze the degree of organic layer damage induced by plasma sputtering through photoluminescence spectroscopy, detailed in Chapters 2 and 3.

**Investigate role of protective layer:** We study the effect of a BPhen (Bathophenanthroline) protective layer, illustrated in Figure 1-2, protective layer employed between organic fluorescent films and ITO.

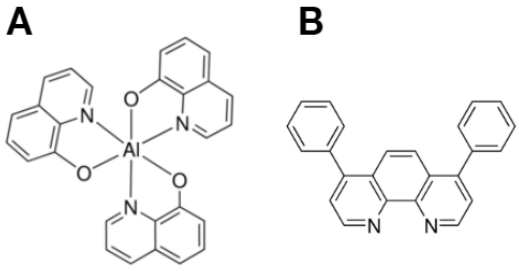



Figure 1-2: Molecular structure of (A) $Alq_3$ (tris(8-hydroxyquinolinato)aluminium) and (B) BPhen (Bathophenanthroline)

**Attempt to isolate damage mechanisms:** We explore the effects of different damage mechanisms by conducting experiments with the shutter open and closed, illustrated in Figure 1-3. This allows us to isolate the gaseous ions, plasma, and electrons exposed to the substrates.

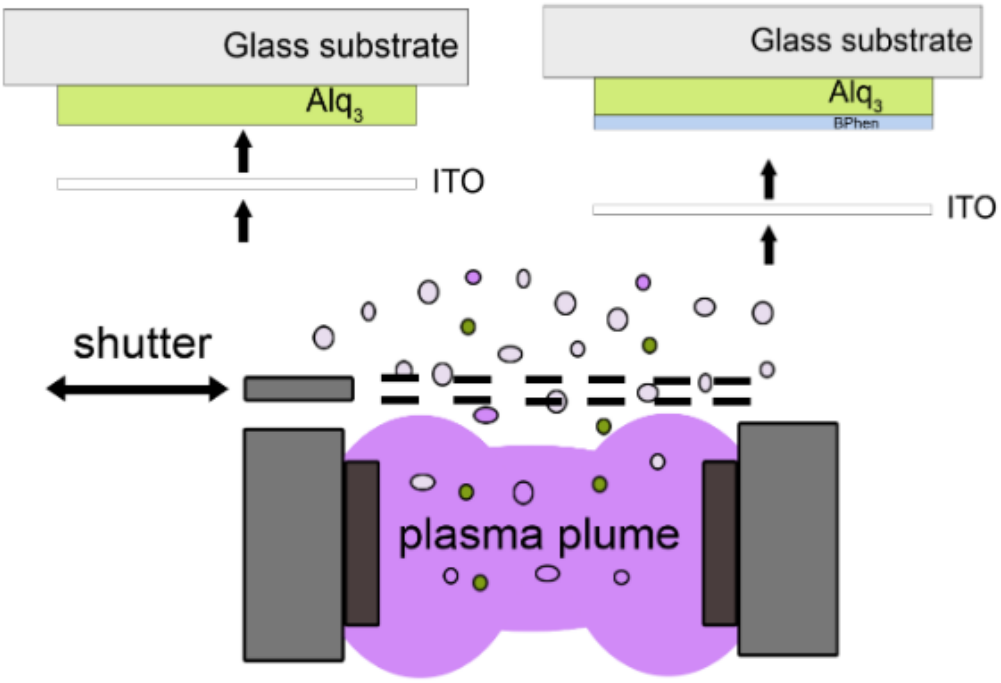



Figure 1-3: Sputter System Shutter State

## 1.4 Summary

The goal of this thesis is to gain an understanding of the damage caused to organic layers when a top ITO electrode is deposited via plasma sputtering. Additionally, this work seeks to explore the effect of plasma sputtering growth rate, as well as the effect of a protective layer. We also isolate certain mechanisms of organic layer damage by observing damage when the plasma is running but with the shutter closed. Through these experiments, we provide a qualitative study of organic damage through methods of photoluminescence spectroscopy.

The theory of plasma sputtering deposition and photoluminescence as a means to characterize sputtering damage is explained in 2. This chapter also contains detailed explanation of mechanisms responsible for organic film damage. Sample fabrication and photoluminescence characterization methods are outlined in 3. The Results of this work are presented in 4, while the Discussion is included in 5. Lastly, the Conclusion outlines opportunities for future research and the impact of this project, 6.

# Chapter 2

# Theory

## 2.1 Plasma Sputter Deposition

Plasma sputter deposition is used to deposit uniform films within a vacuum chamber. For this process, a low pressure vacuum chamber void of additional molecules ensures that unwanted chemical reactions do not occur. Argon is typically used as the inert gas for the plasma due to its low reactivity and abundance. An applied electric field generates a neutral gaseous plasma.

When the high energy ions of the plasma bombard a solid target comprised of the desired film material, these collisions cause the particles from the target material to be ejected and condense on a substrate, forming a thin-film.

Magnetron sputtering systems rely on the Lorentz Force, Equation 2.1, to confine charged particles in the chamber, in which $q$ is the charge of the particle, $\vec{v}$ is the particle's velocity, and $\vec{B}$ is the magnetic field. [26, 27] Figure 2-1 illustrates the configuration of the magnetron sputter system, while Figure 2-2 illustrates the magnet orientation. Previous research suggests that sputtering systems which confine plasma away from the substrates minimize organic film damage. [24, 14, 16, 13, 18]

$$F = q(\vec{v} \times \vec{B}) \tag{2.1}$$

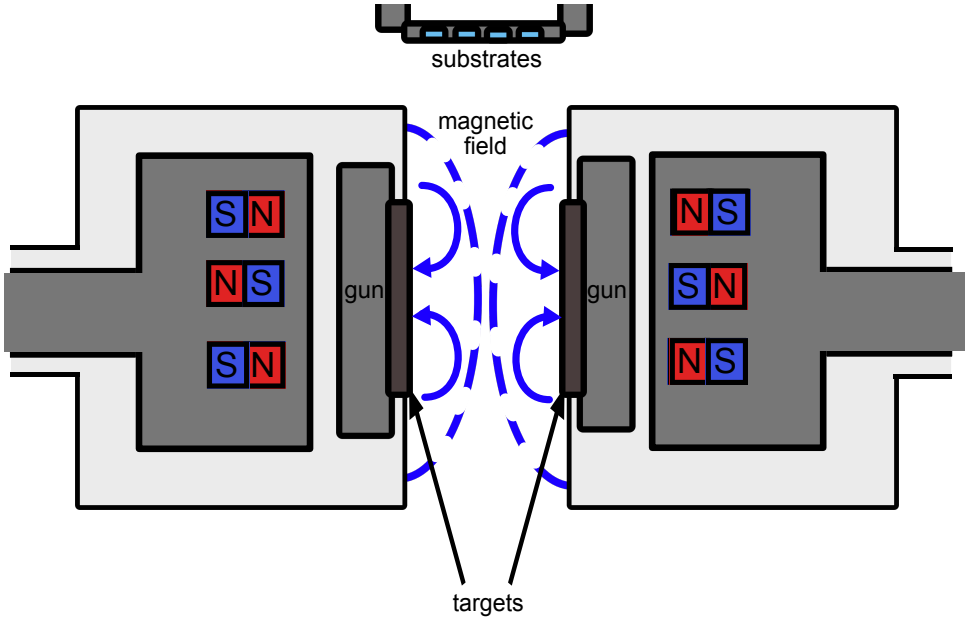



Figure 2-1: Illustration of facing-target magnetron sputter system, where S and N indicate south and north magnetic poles.

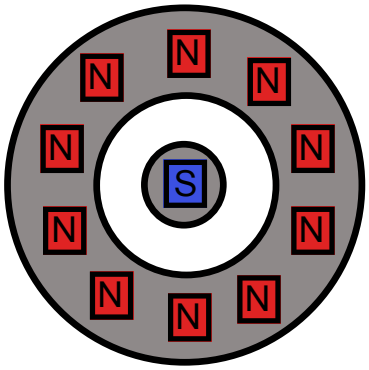



Figure 2-2: Illustration of magnets in gun, from the perspective of the sputter system gun.

To deposit indium tin oxide (ITO) via plasma sputtering, solid ITO targets are bombarded with high energy Argon ions. In facing-target sputtering, the substrate is placed above the plume in effort to reduce damage, illustrated in Figure 2-3. Sputter systems in which the target is placed facing toward the substrates expose films to the plasma plume. This work focuses on films deposited with a sputter system utilizing the magnetron and facing-target design. This thesis explores the cause of damage induced to organic films by plasma sputtering. The various damage mechanisms arising from plasma sputtering are detailed below.

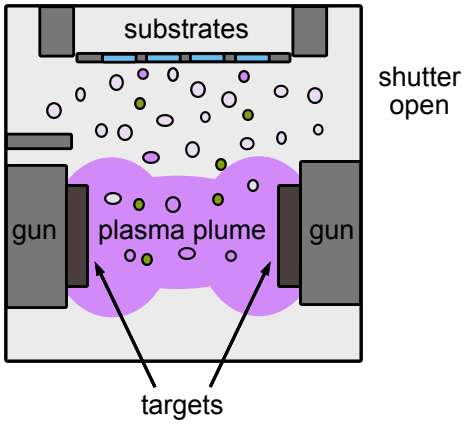



Figure 2-3: Sputter Shutter Open: Gaseous ions, high energy ions and electrons, and secondary electrons can bombard substrates.

## 2.2 Damage Mechanisms

Previous research describes the mechanisms by which organic films are damaged in the process of plasma sputtering. Damage is primarily caused by the bombardment of high energy ITO atoms, neutral Argon atoms, negative oxygen ions, secondary electrons, and plasma irradiation.[24]

Liao et al. simulated the effect of plasma sputtering by exposing $Alq_3$ to an ion beam of 100eV $Ar^+$. They observe significant changes to the surface energy level following ion irradiation at a relatively low energy. They reason that nonradiative recombination in $Alq_3$ result from overlapping gap states between the lowest unoccupied molecular orbital (LUMO) and the highest occupied molecular orbital (HOMO). They propose that the overlapping gap states result in a conductive metal-like $Alq_3$ surface. Researchers estimate that actual electrode deposition will be even more harmful than this controlled experiment. The study concludes that surface damage from sputtering significantly degrades the performance of OLED devices comprised of $Alq_3$ and ITO. [12]

Cheng et al. studied $Alq_3$ films when Argon ion plasma and describe the bond-breaking which occurs in $Alq_3$ upon ion bombardment. They characterized the composition of $Alq_3$ films via XPS and conclude that plasma treatment first broke Al-O and Al-N bonds, forming gases, including CO, $CO_2$, $N_2$, and other organic compounds. [28]

Another study noted the effect of bombardment by electrons. Lei et al. examined the effect of plasma exposure to organic films by studying Photoluminescence (PL) of ion-induced damage to BAlq (Bis(8-hydroxy-2-methylquinoline)-(4-phenylphenoxy)aluminum). They noted a clear decrease in PL intensity upon electron bombardment. [17]

These studies demonstrate that several factors are responsible for damage to $Alq_3$ films. This thesis investigates the effectiveness of the facing-target magnetron sputter system through analysis of organic layer damage with photoluminescence (PL) spectroscopy, described below.

## 2.3 Photoluminescence

Photoluminescence (PL) spectroscopy is a non-contact analytical technique used to probe the electronic structure of materials. When light is aimed at a sample, energy from photons is absorbed by the material, exciting valence electrons to excited electronic states through photoexcitation. Each atomic orbital can hold an electron pair, in which the electrons have opposite spin. The process of photoexcitation conserves electron spin. When electrons return to their equilibrium states following photoexcitation, excess energy is released through the emission of light, or photoluminescence. Photoluminescence spectroscopy measures the number of photons emitted in this process.

Fluorescence describes a type of photoluminescence in which internal energy transitions occur before an electron relaxes from an excited electronic state to a lower electronic state. The internal energy dissipation results in photon emission at a lower energy than the photons absorbed. Thus, the photons emitted have a lower frequency than those absorbed, see Appendix A. Figure 2-4 illustrates fluorescence as an electron relaxes from the excited state, $S_1$, to the ground state, $S_0$, and emits a photon. In Figure 2-4, the electrons are represented by their spin state in blue arrows. [29, 30]

In this study, we utilize PL to study damage caused to an organic fluorescent material, $Alq_3$, by plasma sputtering an ITO film directly on top of $Alq_3$. We would expect the measured Photoluminescence (PL) to decrease with overlap between the low energy and high energy electronic states of $Alq_3$ caused by ion bombardment and irradiation. Thus, we can use PL to measure the degree of $Alq_3$ damage as ITO is sputtered.

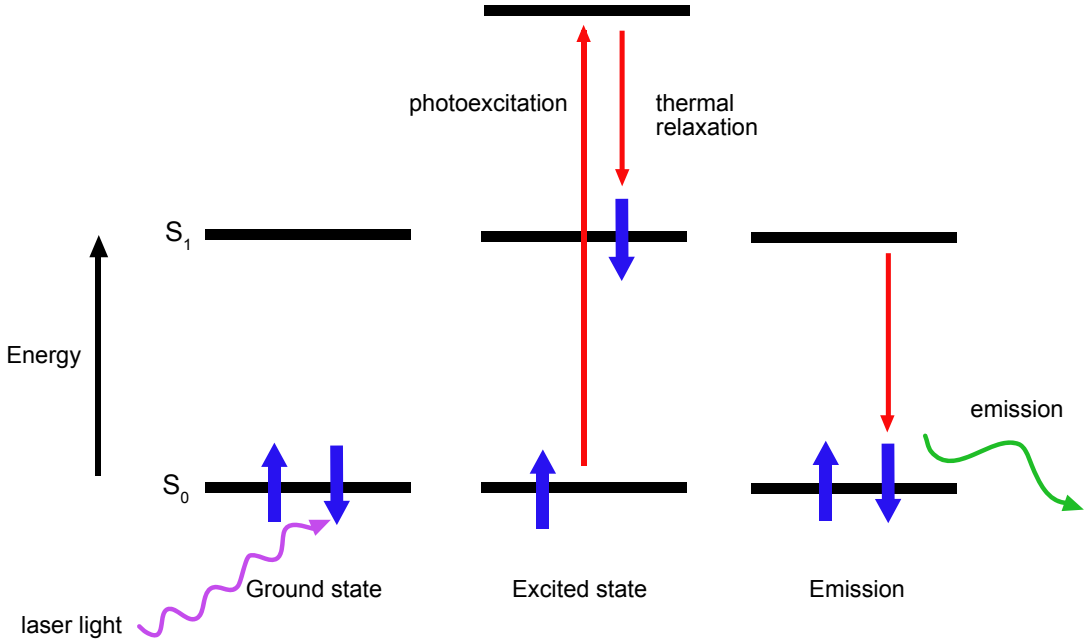



Figure 2-4: Fluorescence: Electrons are represented by their spin state in blue arrows. High energy photons excite an electron from the ground state to an excited state. The electron relaxes to a lower energy state through thermal relaxation. Eventually, as the system reaches equilibrium, the electron relaxes to the ground state and emits a photon of lower energy.

# Chapter 3

# Methods

In this chapter, we provide the details of the fabrication of sample and control structures. We describe the

## 3.1 Fabrication

Glass substrates are cleaned by ultrasonication in a series of solutions. The substrates are placed in an ultrasonic bath in the following solutions for 5 minutes each: (1) Micro-90®, (2) deionized water, (3) acetone, (4) isopropanol. Substrates remain in isopropanol to reduce the introduction of debris as they are transferred into a nitrogen glovebox, which is controlled for oxygen and moisture content . Substrates are removed from isopropanol while laminar flow circulates air in the glovebox to prevent particles from settling on the substrate. Substrates are subsequently dried using a nitrogen spray gun.

Films were deposited on sample and control substrates simultaneously to account for possible variation in film morphology. Organic films were deposited through methods of thermal evaporation. A sample and control film were loaded into a substrate mask in the thermal evaporator chamber and brought to ultra-high vacuum, at a chamber pressure of approximately $1\times10^{-6}$ to $1\times10^{-9}$ Torr. Every control and sample in this study was deposited with 40nm of organic fluorescent $Alq_3$, obtained from Luminescence Technology Corp. The $Alq_3$ film was deposited at approximately 1.8Å/s. Some control and sample structures were deposited with 7nm of BPhen (Bathophenanthroline), obtained from Fisher Scientific, immediately following the deposition of $Alq_3$. Following thermal evaporation, both the sample and control substrates were removed from the chamber. The control was set aside, while the sample was immediately placed into the sputter chamber.

The pressure of the sputter chamber was brought to approximately $1\times10^{-6}$ Torr. The shutter was adjusted to either the closed or open state and the plasma was turned on. For each plasma run, the plasma was initiated at a power of 20W and a pressure of $15\times10^{-3}$ Torr. After the initial strike, the pressure was reduced to $6\times10^{-3}$ Torr and the power was tuned to that required for the desired growth rate.

## 3.2 Plasma Sputter Deposition Trends

In Figure 3-1, we demonstrate that ITO growth rate is linearly related to growth power, with an $R^2$=0.996, for the facing-target sputter system. Thus, to account for fluctuations in the growth rate displayed throughout film deposition, the same growth power is used for samples of the same growth rate.

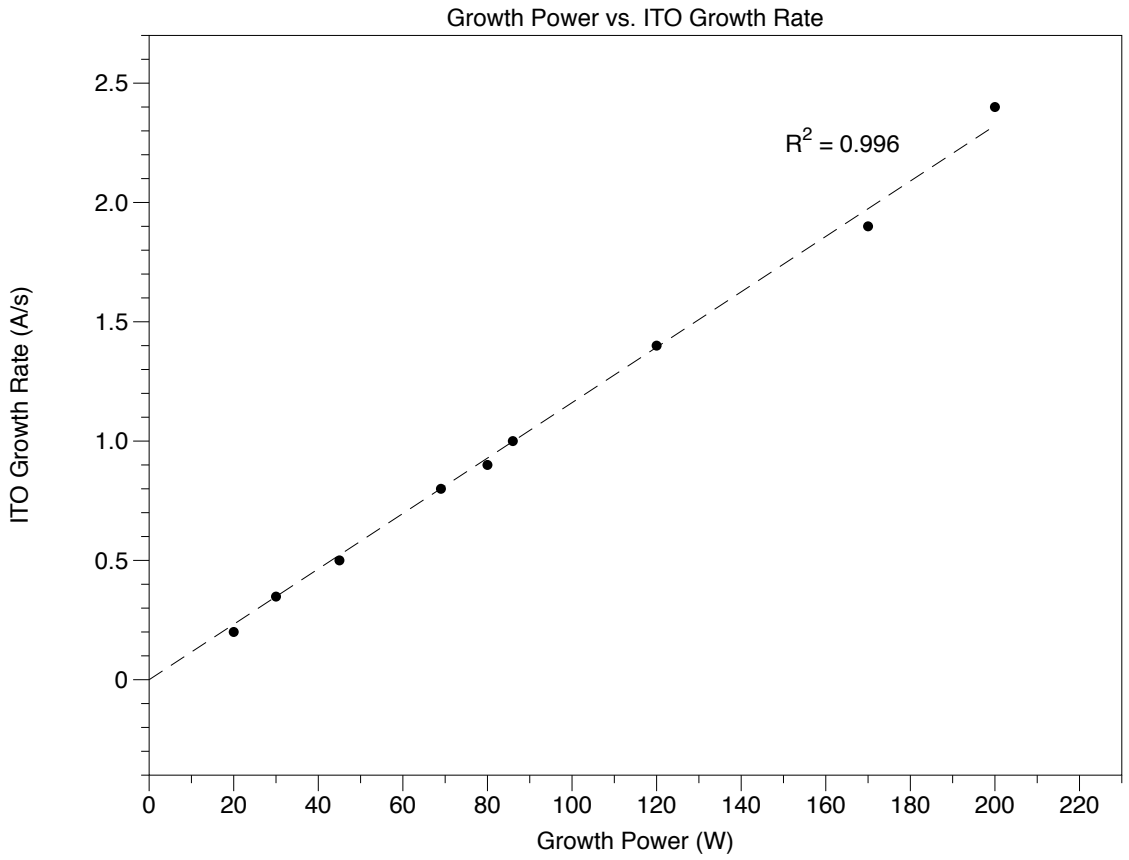



Figure 3-1: Linear Trend Between Growth Rate and Growth Power

## 3.3 Sample and Control Structures

In this study, samples were either deposited with a 10nm ITO film with the shutter open, or samples were placed in the chamber with the shutter closed and plasma running. Tables 3.1, 3.2, 3.3, and 3.4 show the sample and control structures for the ITO film deposition experiment with the shutter open. The tables include the powers and rates considered.

Table 3.1: ITO Deposition Sample Structures Without BPhen

| Structure | Growth Power (W) | Growth Rate (Å/s) |
|---|---|---|
| glass/$Alq_3$(40nm)/ITO(10nm) | 20 | 0.2 |
| glass/$Alq_3$(40nm)/ITO(10nm) | 45 | 0.5 |
| glass/$Alq_3$(40nm)/ITO(10nm) | 69 | 0.8 |
| glass/$Alq_3$(40nm)/ITO(10nm) | 80 | 0.9 |
| glass/$Alq_3$(40nm)/ITO(10nm) | 86 | 1.0 |
| glass/$Alq_3$(40nm)/ITO(10nm) | 120 | 1.4 |
| glass/$Alq_3$(40nm)/ITO(10nm) | 170 | 1.9 |
| glass/$Alq_3$(40nm)/ITO(10nm) | 200 | 2.4 |

Table 3.2: ITO Deposition Control Structures Without BPhen

| Structure | Growth Power (W) | Growth Rate (Å/s) |
|---|---|---|
| glass/$Alq_3$(40nm) | 20 | 0.2 |
| glass/$Alq_3$(40nm) | 45 | 0.5 |
| glass/$Alq_3$(40nm) | 69 | 0.8 |
| glass/$Alq_3$(40nm) | 80 | 0.9 |
| glass/$Alq_3$(40nm) | 86 | 1.0 |
| glass/$Alq_3$(40nm) | 120 | 1.4 |
| glass/$Alq_3$(40nm) | 170 | 1.9 |
| glass/$Alq_3$(40nm) | 200 | 2.4 |

Table 3.3: ITO Deposition Sample Structures With BPhen

| Structure | Growth Power (W) | Growth Rate (Å/s) |
|---|---|---|
| glass/$Alq_3$(40nm)/BPhen(7nm)/ITO(10nm) | 20 | 0.2 |
| glass/$Alq_3$(40nm)/BPhen(7nm)/ITO(10nm) | 45 | 0.5 |
| glass/$Alq_3$(40nm)/BPhen(7nm)/ITO(10nm) | 69 | 0.8 |
| glass/$Alq_3$(40nm)/BPhen(7nm)/ITO(10nm) | 80 | 0.9 |
| glass/$Alq_3$(40nm)/BPhen(7nm)/ITO(10nm) | 86 | 1.0 |
| glass/$Alq_3$(40nm)/BPhen(7nm)/ITO(10nm) | 120 | 1.4 |
| glass/$Alq_3$(40nm)/BPhen(7nm)/ITO(10nm) | 170 | 1.9 |
| glass/$Alq_3$(40nm)/BPhen(7nm)/ITO(10nm) | 200 | 2.4 |

Table 3.4: ITO Deposition Control Structures With BPhen

| Structure | Growth Power (W) | Growth Rate (Å/s) |
|---|---|---|
| glass/$Alq_3$(40nm)/BPhen(7nm) | 20 | 0.2 |
| glass/$Alq_3$(40nm)/BPhen(7nm) | 45 | 0.5 |
| glass/$Alq_3$(40nm)/BPhen(7nm) | 69 | 0.8 |
| glass/$Alq_3$(40nm)/BPhen(7nm) | 80 | 0.9 |
| glass/$Alq_3$(40nm)/BPhen(7nm) | 86 | 1.0 |
| glass/$Alq_3$(40nm)/BPhen(7nm) | 120 | 1.4 |
| glass/$Alq_3$(40nm)/BPhen(7nm) | 170 | 1.9 |
| glass/$Alq_3$(40nm)/BPhen(7nm) | 200 | 2.4 |

Tables 3.5 and 3.6 show the sample and control structures for the experiment in which the shutter was closed during the plasma sputtering process. As with the other experiment, we considered samples fabricated with various ITO growth rates.

Table 3.5: Gaseous Ion Exposure Sample and Control Structures Without BPhen

| Structure | Growth Power (W) | Growth Rate (Å/s) |
|---|---|---|
| glass/$Alq_3$(40nm) | 20 | 0.2 |
| glass/$Alq_3$(40nm) | 80 | 0.9 |
| glass/$Alq_3$(40nm) | 200 | 2.4 |

Table 3.6: Gaseous Ion Exposure Sample and Control Structures With BPhen

| Structure | Growth Power (W) | Growth Rate (Å/s) |
|---|---|---|
| glass/$Alq_3$(40nm)/BPhen(7nm) | 20 | 0.2 |
| glass/$Alq_3$(40nm)/BPhen(7nm) | 80 | 0.9 |
| glass/$Alq_3$(40nm)/BPhen(7nm) | 200 | 2.4 |

## 3.4 Photoluminescence Analysis Techniques

The samples and controls were analyzed within Nitrogen gloveboxes. The substrates were placed in the same orientation on a stage and illuminated with a standard green laser diode with a wavelength of 532nm, see Figure 3-2. Fluorescence was measured using FilmTek$^{TM}$ software. We attempted to use the same laser position, angle, and intensity for each measurement. Three PL measurements were taken in the center of each sample and control. We would expect a 1-5% measurement accuracy assuming negligible spectral and chemical interferences. [30]

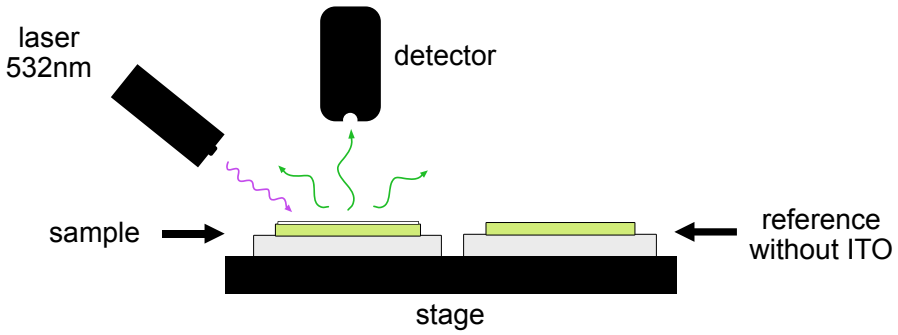



Figure 3-2: Photoluminescence Spectroscopy Setup

The average of measured PL spectra was calculated from the three measurements. The damage was assessed through calculating the Normalized PL, Equation 3.1, using PL measurements of the sample and control, demonstrated in Figure 3-3. This allowed us to compare the PL of $Alq_3$ before and after either plasma sputtering. These calculations as well as their associated error propagation are included in Appendix A.

$$\text{Normalized PL} = \frac{\text{Sample Average Maximum PL}}{\text{Control Average Maximum PL}} \tag{3.1}$$

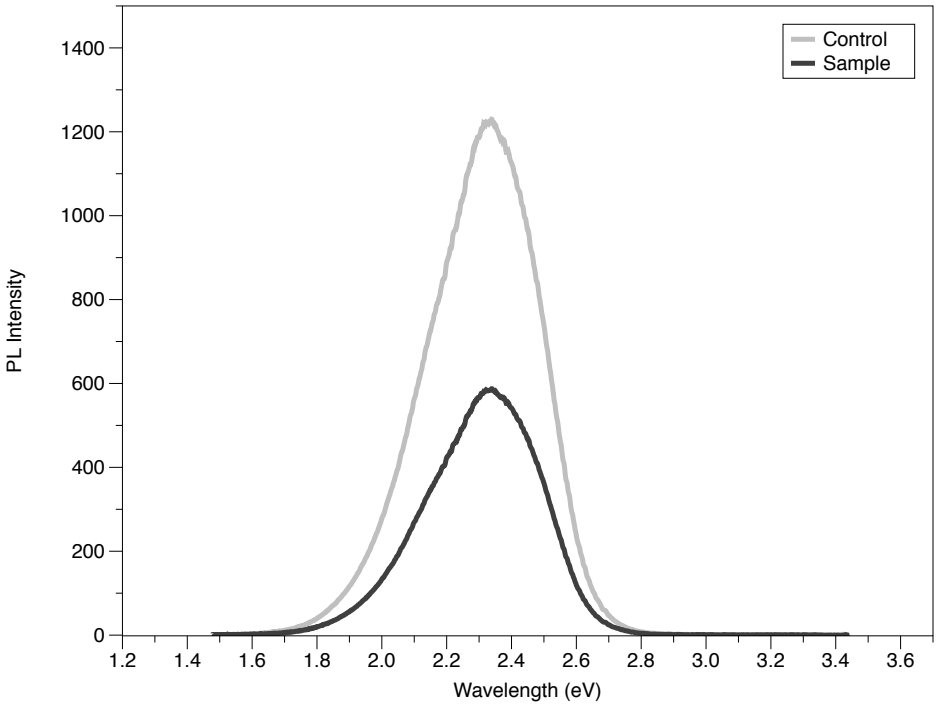



Figure 3-3: PL: Sample and Control Measurements

# Chapter 4

# Results

This chapter presents an assessment of organic film damage through measuring Photoluminescence (PL). To investigate the effect of depositing an ITO film on an organic material, we considered the PL of fluorescent $Alq_3$ (tris(8-hydroxyquinolinato)aluminium).

Sample structures are presented in Tables 4.1 and 4.2. Figures 4-1, 4-2, 4-5, and 4-6 illustrate the sample structures considered in this study. Normalized PL as a function of growth rate is presented along with normalized PL spectra.

## 4.1 Effect of ITO Film Deposition on Organic Film Damage

### 4.1.1 Effect of Depositing ITO on a Fluorescent Organic Layer

We fabricated structures of $Alq_3$ and ITO on glass, illustrated in Figure 4-2. Multiple samples were fabricated to measure PL as a function of growth rate, included in Table 4.1. A control film, Figure 4-1, consisting of only $Alq_3$ was created for each sample. As described in Chapter 3, the PL was measured for both sample and control to calculate the normalized PL for various ITO growth rates.




Figure 4-1: Structure: glass / 40nm $Alq_3$

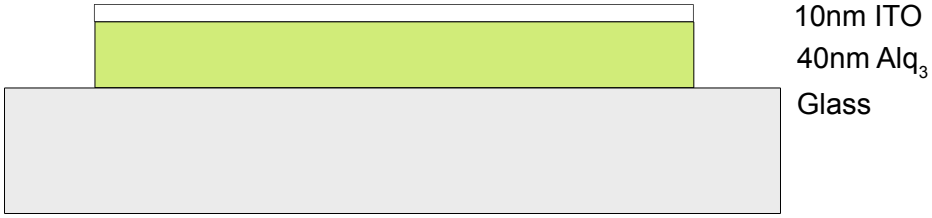



Figure 4-2: Structure: glass / 40nm $Alq_3$ / 10nm ITO

Table 4.1: ITO Deposition Sample Structures

| Structure | Growth Power (W) | Growth Rate (Å/s) |
|---|---|---|
| glass/$Alq_3$(40nm)/ITO(10nm) | 20 | 0.2 |
| glass/$Alq_3$(40nm)/ITO(10nm) | 45 | 0.5 |
| glass/$Alq_3$(40nm)/ITO(10nm) | 69 | 0.8 |
| glass/$Alq_3$(40nm)/ITO(10nm) | 80 | 0.9 |
| glass/$Alq_3$(40nm)/ITO(10nm) | 86 | 1.0 |
| glass/$Alq_3$(40nm)/ITO(10nm) | 120 | 1.4 |
| glass/$Alq_3$(40nm)/ITO(10nm) | 170 | 1.9 |
| glass/$Alq_3$(40nm)/ITO(10nm) | 200 | 2.4 |

For Figure 4-3, each data point represents a PL ratio calculated from Equation 4.1 as detailed in Chapter 3.

$$\text{Normalized PL} = \frac{\text{Average PL Maximum With ITO}}{\text{Average PL Maximum Without ITO}} \tag{4.1}$$

Figure 4-3 shows normalized PL decreases with increasing ITO growth rate when ITO is deposited on $Alq_3$. The normalized PL ranges from approximately 0.48 to 0.58. Therefore, the difference in normalized PL between the lowest ITO growth rate, 0.2Å/s, and the highest, 2.4Å/s, is 0.1. This is highlighted in the plot of PL spectra at these rates, Figure 4-4.

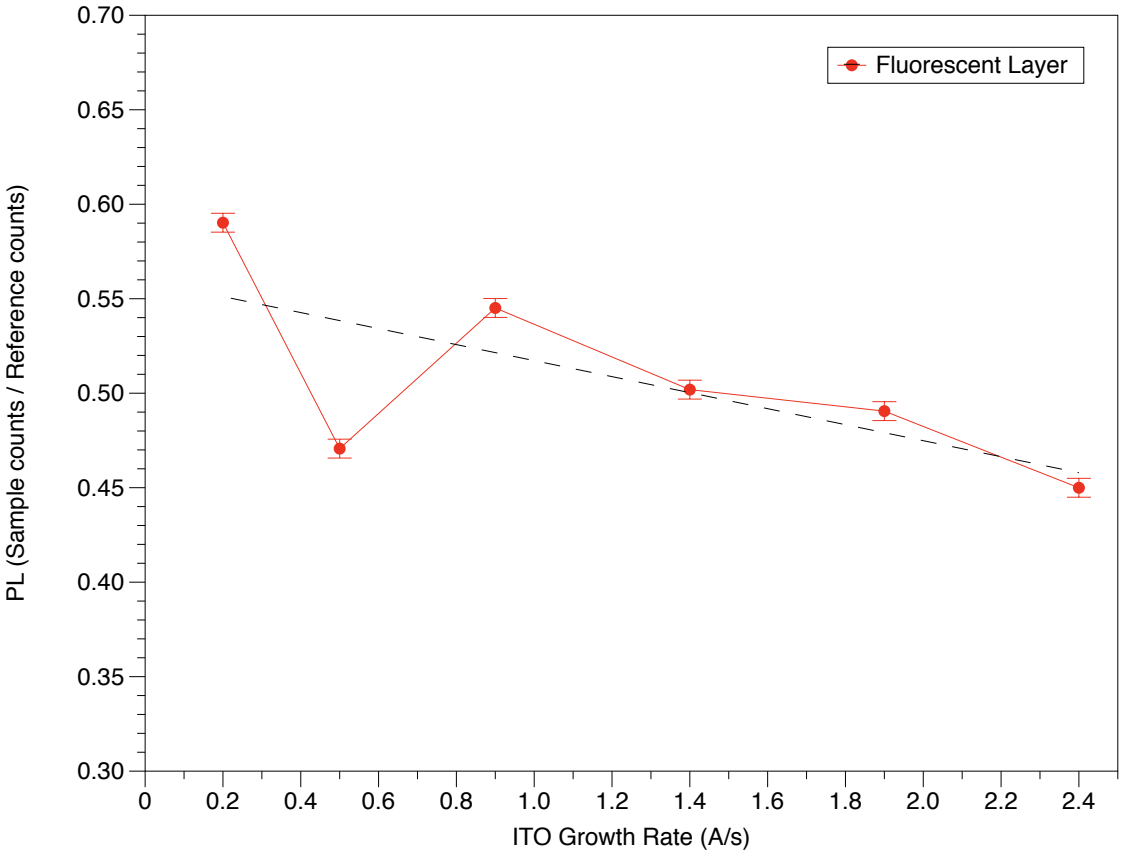



Figure 4-3: ITO Film Without BPhen Protective Layer

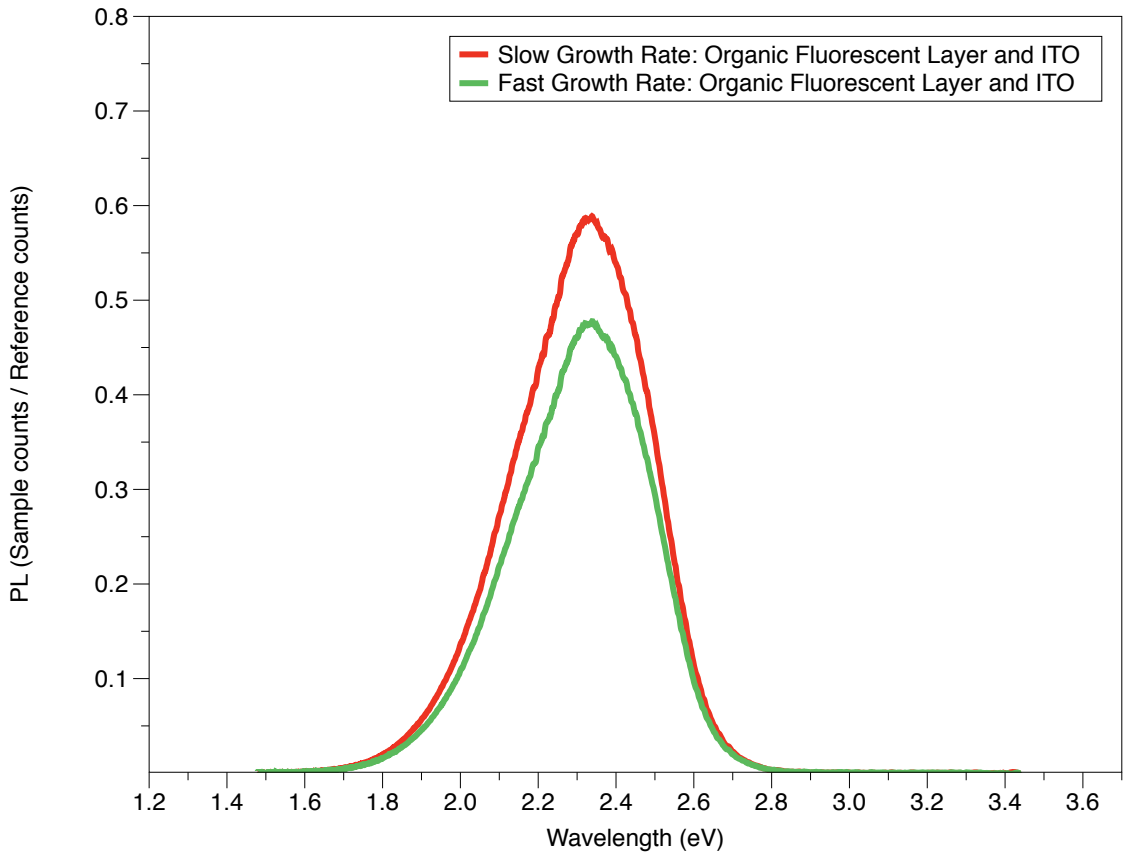



Figure 4-4: PL Spectra: glass / 40nm $Alq_3$ / 100nm ITO

A normalized PL difference of approximately 0.1 is minimal, representing only a 10% difference in $Alq_3$ PL between the samples with highest and lowest ITO growth rate. This suggests that the $Alq_3$ film is not damaged to a greater degree at a high growth rate than a low growth rate. However, this does not account for the primary damage mechanism that governs the degradation of $Alq_3$ during the plasma sputtering process. The sample sputtered at the lowest rate of 0.2Å/s has the highest normalized PL value at 0.6. However, this means that the photoluminescence of the $Alq_3$ is only 60% of the value before ITO deposition.

In an effort to investigate the mechanism responsible for $Alq_3$ film damage, we considered the role of a protective layer between $Alq_3$ and ITO.

### 4.1.2 Effect of Depositing ITO on a Fluorescent Organic Layer with Protective Buffer Layer

We considered the effect of ITO growth rate on PL when a protective layer was employed between $Alq_3$ and ITO. Figures 4-5 and 4-6 illustrate the control and sample structures. ITO was deposited at eight growth rates, from 0.2Å/s to 2.4Å/s, as illustrated in Table 4.2.

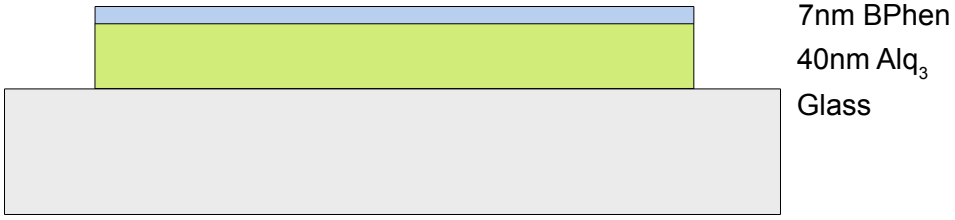



Figure 4-5: Structure: glass / 40nm $Alq_3$ / 7nm BPhen

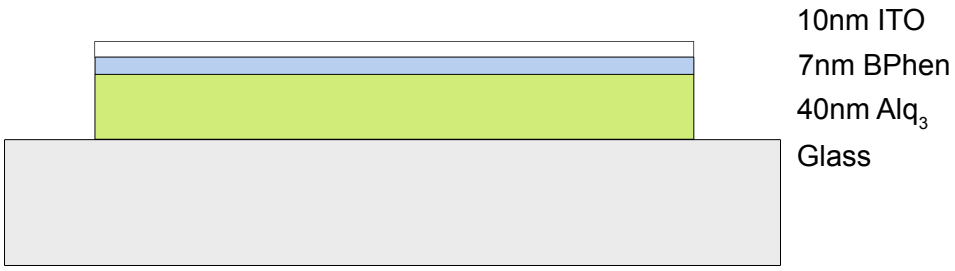



Figure 4-6: Structure: glass / 40nm $Alq_3$ / 7nm BPhen / 10nm ITO

Table 4.2: ITO Deposition Sample Structures With BPhen

| Structure | Growth Power (W) | Growth Rate (Å/s) |
|---|---|---|
| glass/$Alq_3$(40nm)/BPhen(7nm)/ITO(10nm) | 20 | 0.2 |
| glass/$Alq_3$(40nm)/BPhen(7nm)/ITO(10nm) | 45 | 0.5 |
| glass/$Alq_3$(40nm)/BPhen(7nm)/ITO(10nm) | 69 | 0.8 |
| glass/$Alq_3$(40nm)/BPhen(7nm)/ITO(10nm) | 80 | 0.9 |
| glass/$Alq_3$(40nm)/BPhen(7nm)/ITO(10nm) | 86 | 1.0 |
| glass/$Alq_3$(40nm)/BPhen(7nm)/ITO(10nm) | 120 | 1.4 |
| glass/$Alq_3$(40nm)/BPhen(7nm)/ITO(10nm) | 170 | 1.9 |
| glass/$Alq_3$(40nm)/BPhen(7nm)/ITO(10nm) | 200 | 2.4 |

Figure 4-7 shows normalized PL decreases with increasing ITO growth rate. The normalized PL does not show significant variation from that of the structures without a BPhen protective layer, demonstrated in Figure 4-3.

Additionally, Figure 4-17 shows the normalized PL spectra as measured at the extremes of the growth rates considered. Again, there is a minimal difference in peak PL. For these samples with the protective BPhen layer, the difference in maximum PL between a growth rate of 0.2Å/s and 2.4Å/s is approximately 0.15.

The similarity in results presented in this section and the section above indicate that BPhen does not protect against the damage induced to $Alq_3$ when an ITO film is deposited. Additionally, a BPhen layer does not have a significant effect on PL for samples sputtered with a high or low growth rate.

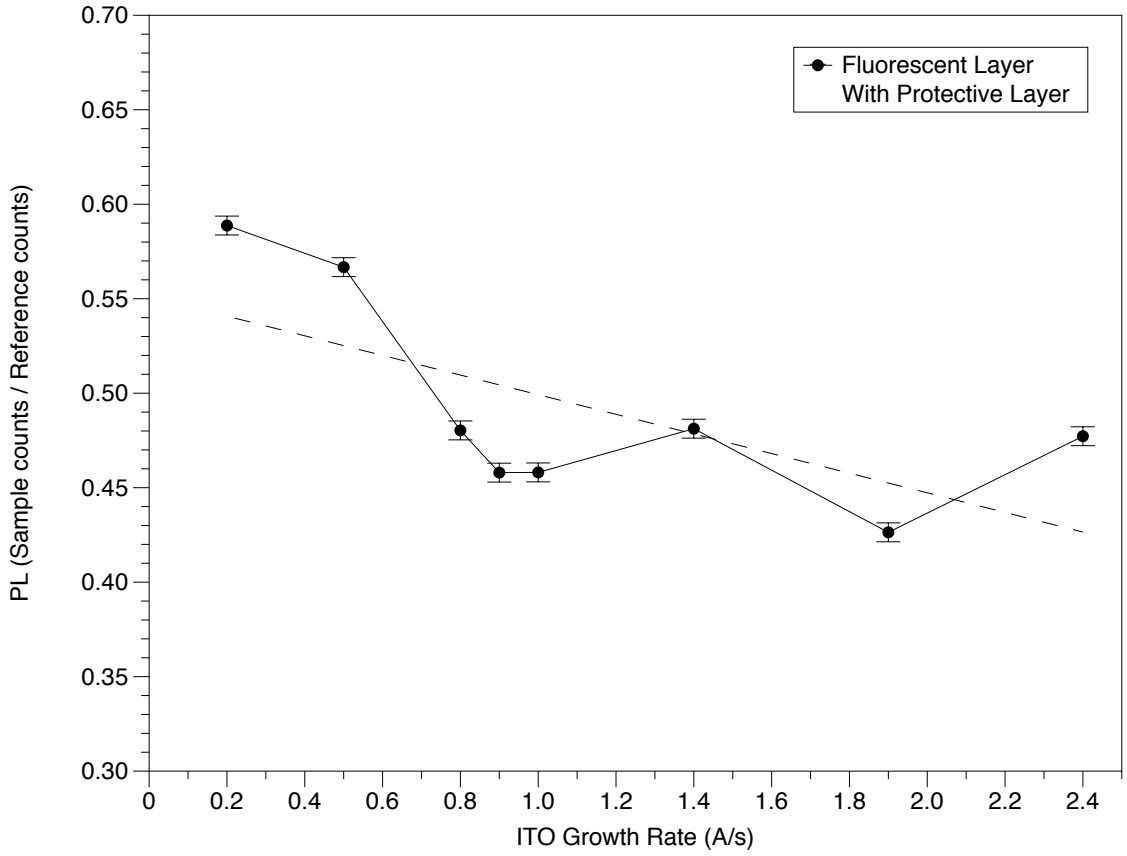



Figure 4-7: ITO Film Deposition With BPhen Protective Layer

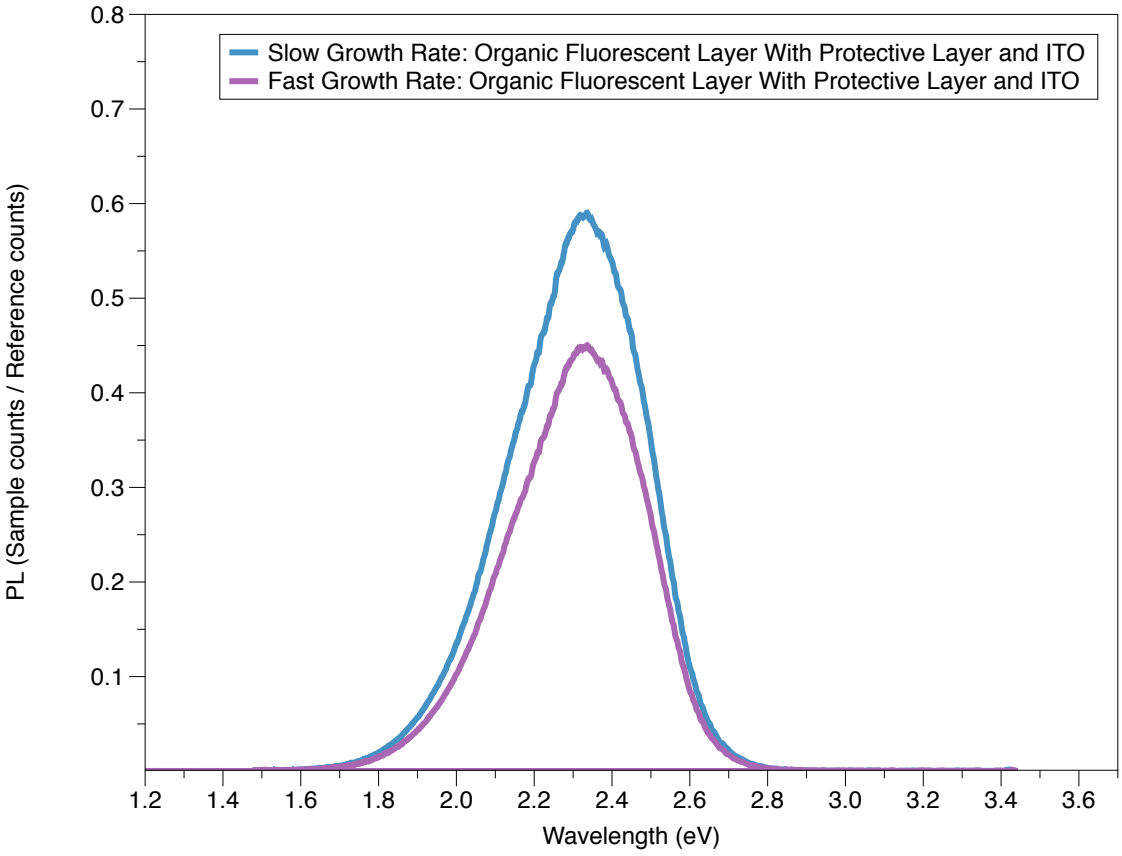



Figure 4-8: PL Spectra: glass / 40nm $Alq_3$ / 7nm BPhen / 100nm ITO

### 4.1.3 Consistent Organic Damage

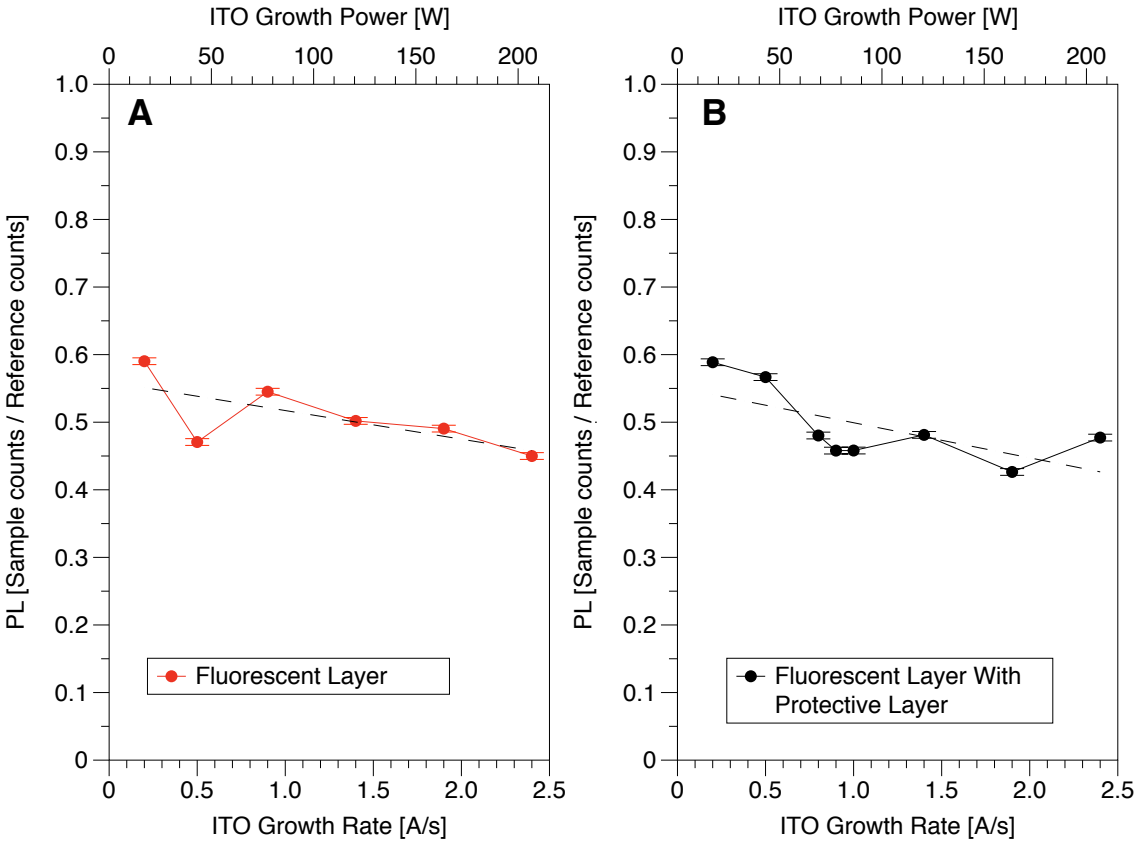



Figure 4-9: ITO Deposition: Growth Rate vs. PL Ratio Comparison

These two experiments are summarized in Figure 4-9. Plots A and B show that PL decreases slightly with increasing growth rate.

Figure 4-10 shows a comparison of the normalized PL spectra at the minimum and maximum growth rates considered for structures of glass / $Alq_3$ / ITO as well as glass / $Alq_3$ / BPhen / ITO. There is negligible difference between spectra for structures with and without a BPhen protective layer. Additionally, the difference in peak PL intensity between the high rate and low rate is approximately 0.1-0.15, meaning there is a 10-15% difference between structures with ITO deposited at a low and structures with ITO deposited at a high rate.

This suggests that a BPhen protective layer does not change the amount of organic layer damage which occurs at different growth rates. This implies that additional factors separate from ITO growth rate account for the damage which caused $Alq_3$

films to decrease in PL by 40-55% of the original value following ITO deposition.

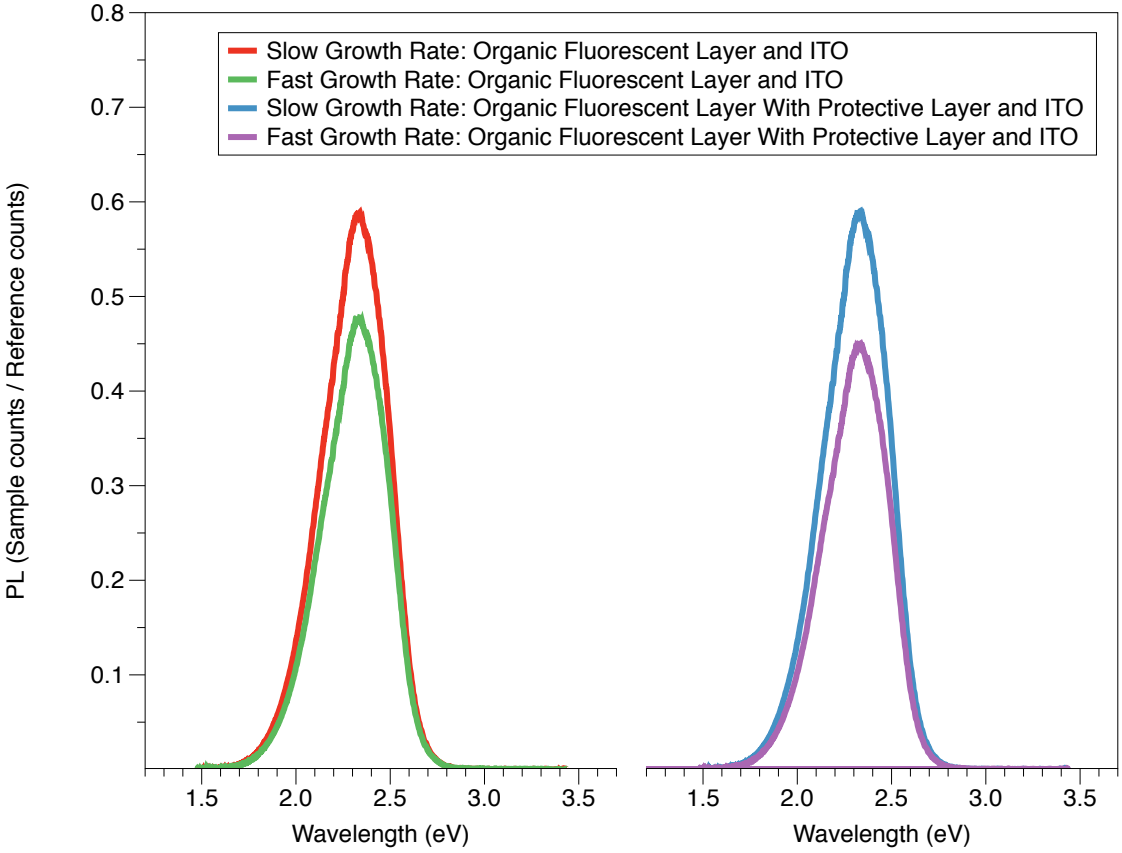



Figure 4-10: ITO Deposition: PL Spectra Comparison

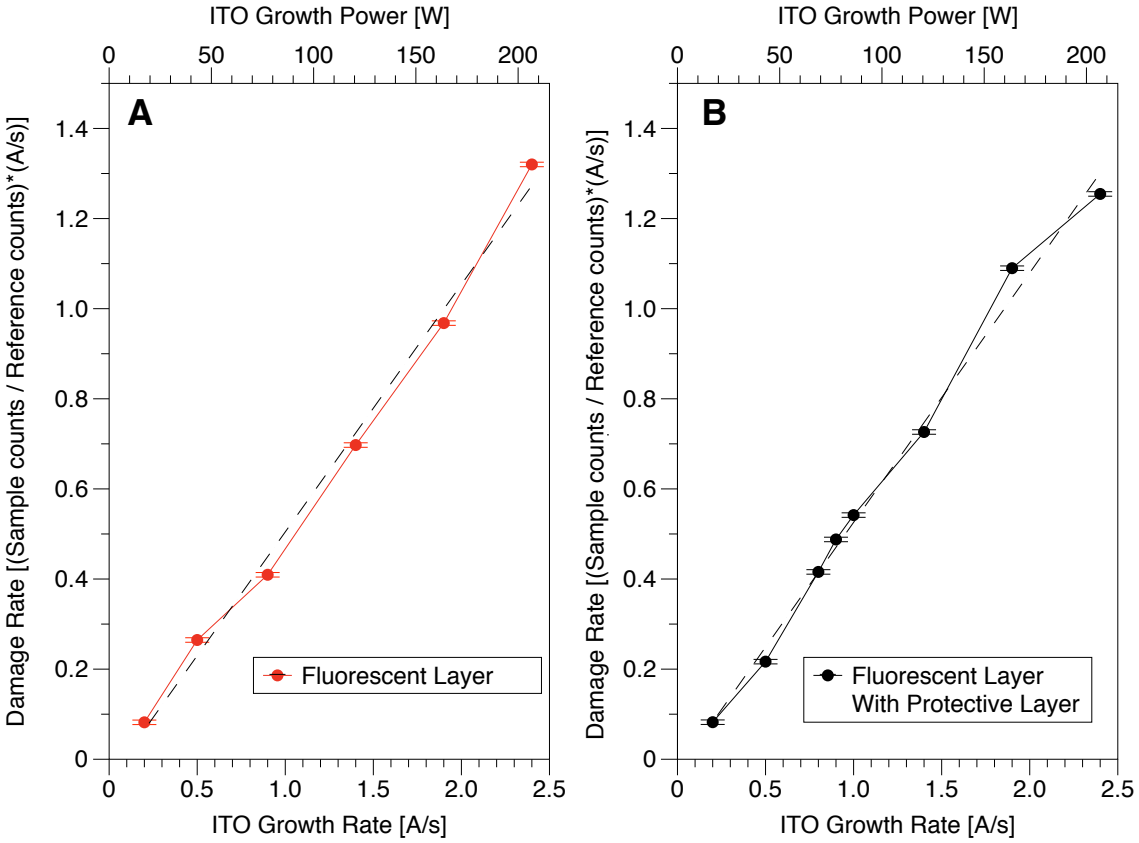



Figure 4-11: ITO Deposition: Illustrating Damage Rate vs. ITO Growth Rate

Figure 4-11 shows the damage rate, Equation 4.2, as a function of ITO growth rate. The slope of the line connecting the data points represents damage. For plots A and B, the slope does not vary widely as a function of growth rate.

$$\text{Damage Rate} = (1 - \text{PL}) * (\text{ITO Growth Rate}) \tag{4.2}$$

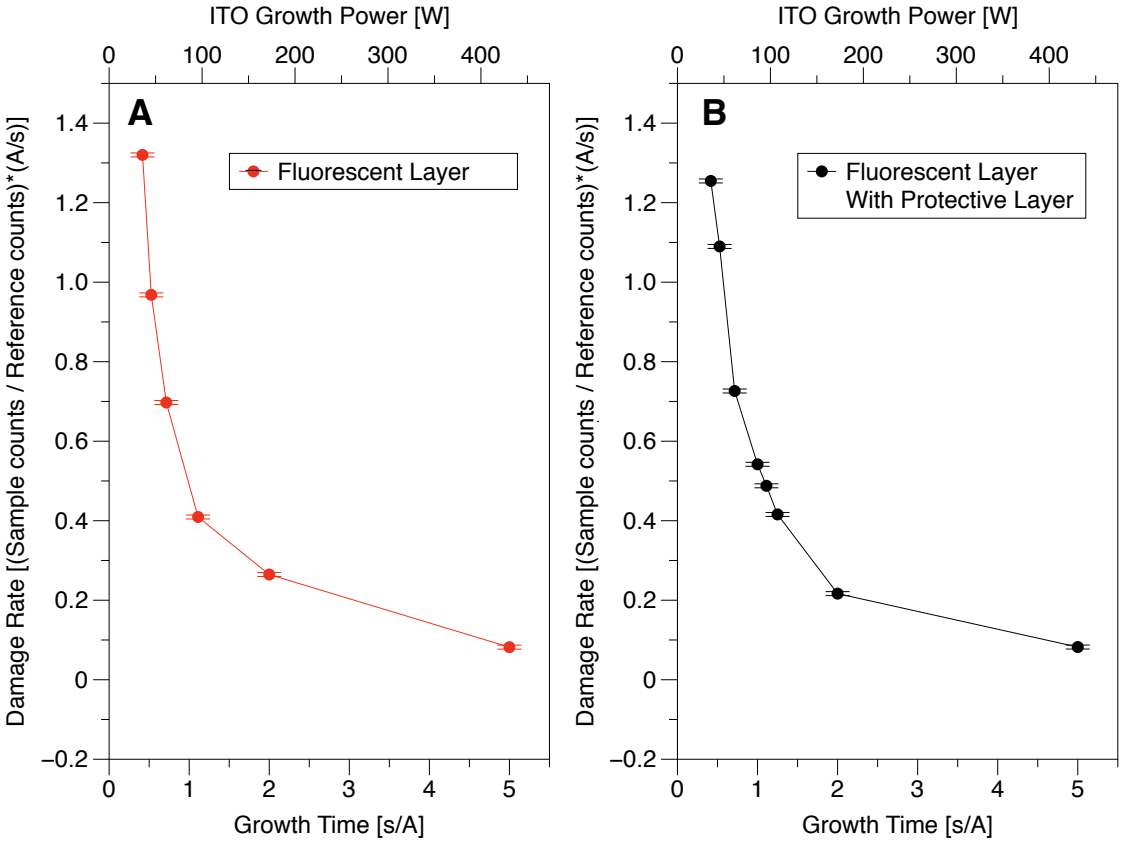



Figure 4-12: ITO Deposition: Illustrating Damage Rate vs. Growth Time

Figure 4-12 shows damage rate as a function of growth time, Equation 4.3. For these plots, the area under the curve represents damage. Plots A and B demonstrate that greater damage occurs at the beginning of ITO film growth.

$$\text{Growth Time} = \frac{1}{\text{ITO Growth Rate}} \tag{4.3}$$

## 4.2 Plasma Sputter Shutter State

We designed experiments to explore damage mechanisms separate from high energy ion and electron collisions when an ITO film is deposited. To explore the effect of exposure to gas from the chamber on $Alq_3$ films, we altered the state of the shutter which separates the substrates from the plasma sputtering chamber. In the closed state, an aluminum sheet shields substrates from the plasma sputtering process below, while in the open state, the aluminum sheet is an a retracted state to the side of the substrates, exposing them to ions from the plasma sputtering below. ITO film is deposited with the shutter open so ITO material can grow on the substrates.

Our results detailed above suggest that ITO growth rate has little effect on $Alq_3$ damage, with little variation between the lowest and highest growth rates. In the following section, we present a study to investigate the effect of exposure to gaseous ions which would not be shielded from the substrates by the shutter.

Therefore, the experiment presented in the section above constitute the results of plasma sputtering conducted when the shutter is in the open state, necessary for ITO film deposition. The section below describes an investigation of the effect of an open shutter, where $Alq_3$ is exposed to gaseous ions.

## 4.3 Effect of Gaseous Ion Exposure

We considered the effect of exposure to gaseous ions for sample structures of glass/$Alq_3$ and for structures of glass/$Alq_3$/BPhen, illustrated in Figures 4-13 and 4-14. We sought to determine whether BPhen served to protect $Alq_3$ upon exposure to gaseous ions.

The samples were exposed to ozone at three rates, 0.2Å/s, 0.9Å/s, and 2.4Å/s. The samples were placed in the substrate holder and the plasma sputtering process was identical to that executed for samples deposited with an ITO film. However, in this case, the shutter was closed.




Figure 4-13: Structure: glass / 40nm $Alq_3$

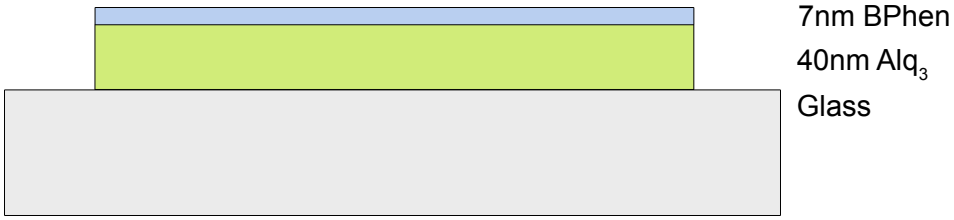



Figure 4-14: Structure: glass / 40nm $Alq_3$ / 7nm BPhen

Figure 4-15 shows normalized PL as a function of ITO growth rate for samples exposed to gaseous ions with a closed shutter. For the samples without BPhen, there is a higher normalized PL for those exposed to gaseous ions produced upon sputtering at 0.2Å/s compared to the rate of 2.4Å/s. However, for structures with a BPhen protective layer, there is not a decrease in normalized PL with increasing growth rate.

Figures 4-16 and 4-17 illustrate these PL spectra trends. Figure 4-16 shows the normalized peak PL decreases with increasing growth rate for structures without BPhen, while Figure 4-17 shows an increase in normalized peak PL with increasing rate.

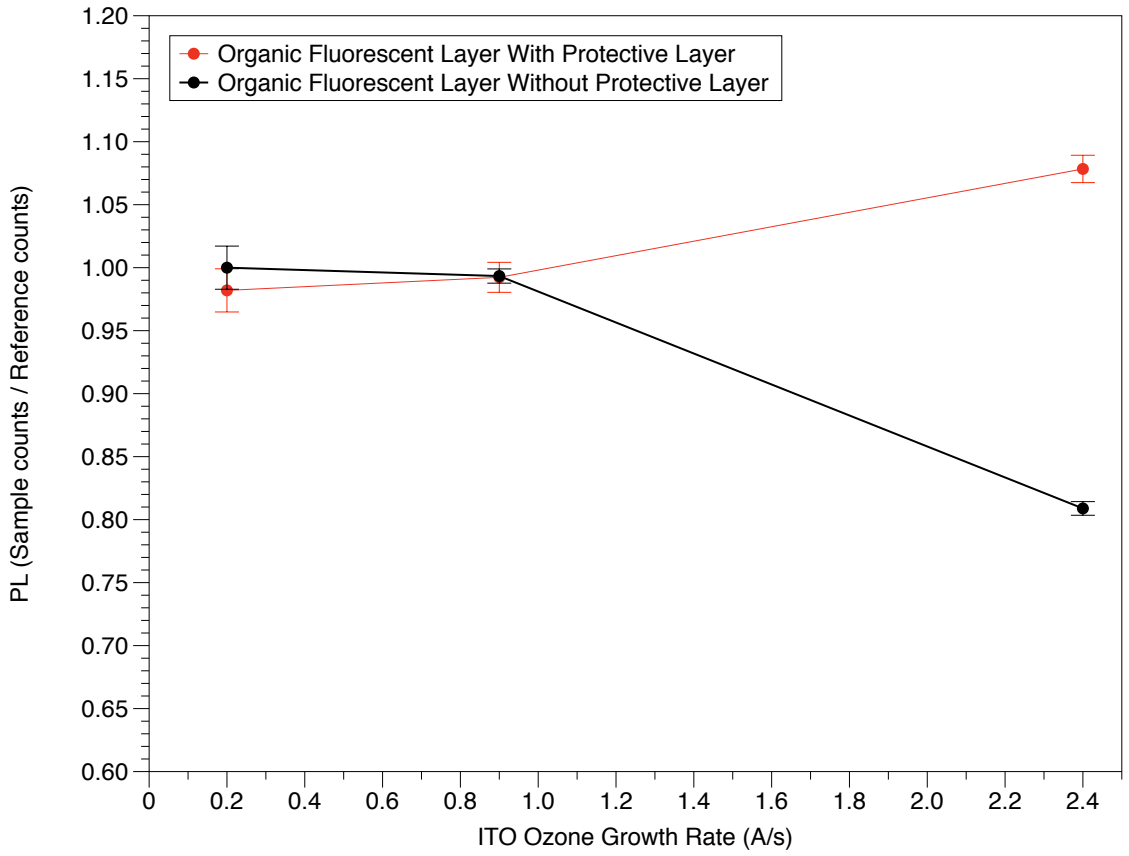



Figure 4-15: Gaseous Ion Exposure With and Without BPhen Protective Layer

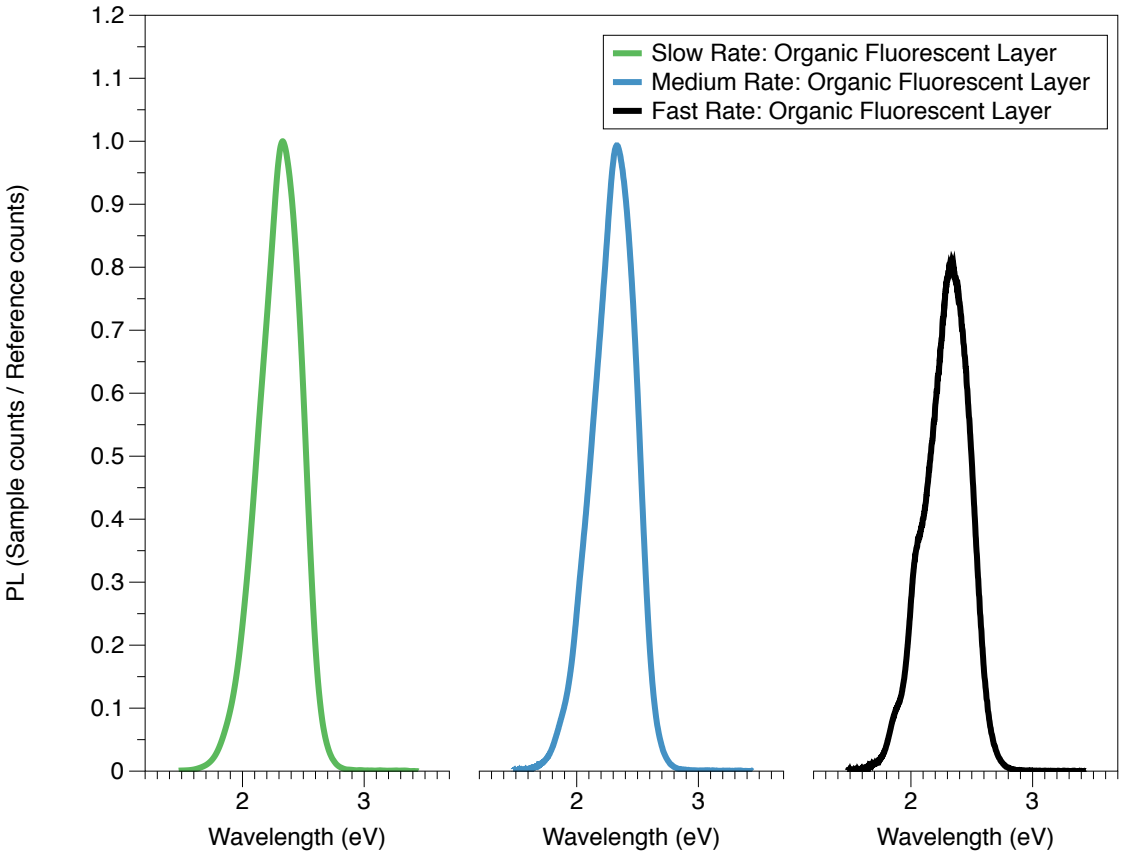



Figure 4-16: PL Spectra: Gaseous Ion Exposure Without BPhen Protective Layer

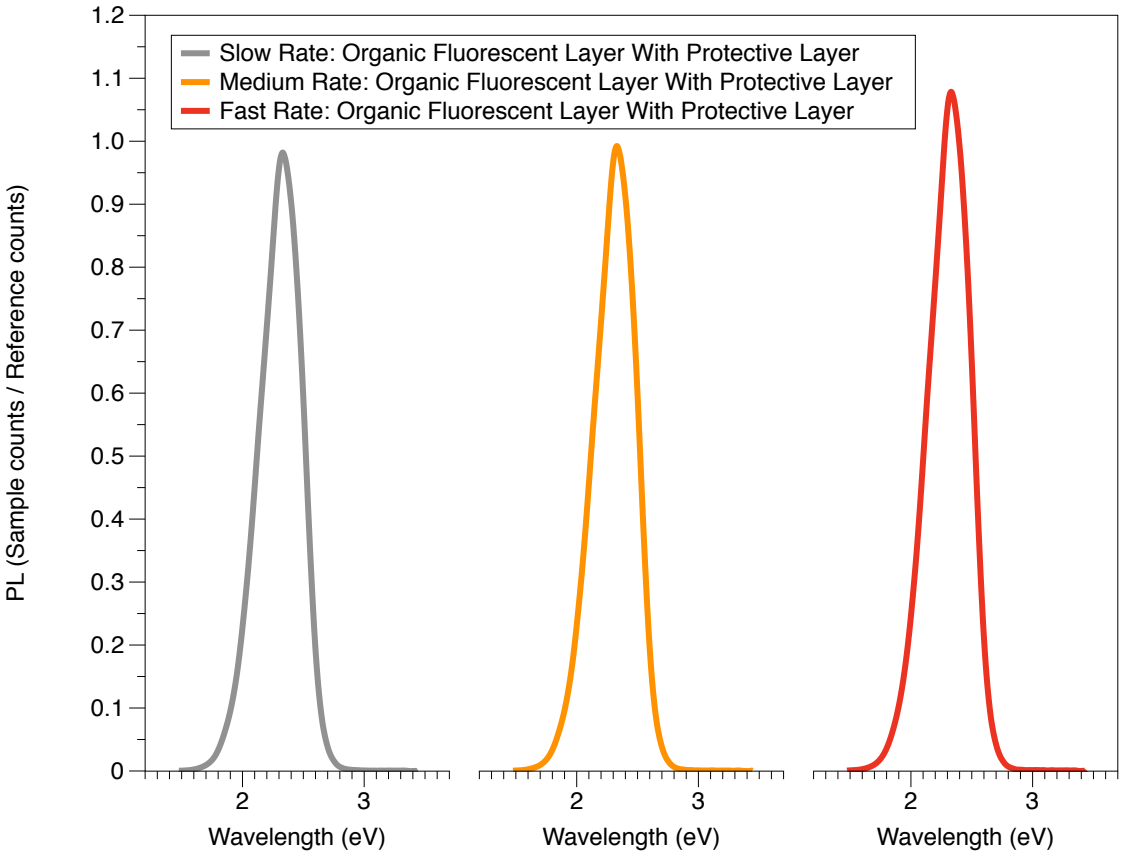



Figure 4-17: PL Spectra: Gaseous Ion Exposure With BPhen Protective Layer

## 4.4 Summary of Results

In this chapter, we described the results of PL damage analysis for structures deposited with ITO as well as structures exposed only to gaseous ions. We show that PL is not strongly affected by growth rate for structures deposited with ITO. Our findings illustrate that greater organic film damage occurs at the start of sputtering. We demonstrate that BPhen protects against $Alq_3$ damage at high rates. In Chapter 5, we will explore the factors responsible for the reductions in PL.

# Chapter 5

# Discussion

In Chapter 4, we present results of PL measured for samples exposed to the plasma sputtering process. This chapter offers a discussion on the nature of the facing-target sputter system and the effect of growth rate. Additionally, we explore possible mechanisms responsible for damage, described in Chapter 4, at various stages of plasma sputtering the experiments and the controls adopted to address potential sources of error.

## 5.1 Facing-Target Sputtering System

Previous work suggests that facing-target magnetron sputter systems prevent film damage by reducing bombardment from secondary electrons and negatively-charged oxygen ions more effectively than systems that operate at low voltage or use a conventional target configuration. [13, 14, 16, 18, 24]

This work was performed with a facing-target sputter system tailored for low-damage film deposition designed by Sophia Weeks. [23] Conventional sputter systems in which substrates are exposed to the plasma plume may not allow for detailed analysis of the damage mechanisms responsible for degradation of organic films.

## 5.2 Growth Rate

Lei et al. investigated the effect of plasma sputtering ITO on BAlq (Bis(8-hydroxy-2-methylquinoline)-(4-phenylphenoxy)aluminum) films using facing-target sputtering and by analyzing PL from BAlq. The paper concluded that reducing high energy electron bombardment to the substrate was key to mitigating BAlq damage. [11]

Other researchers have cited the collision of high-energy ion and electrons with $Alq_3$ as primary damage mechanism. For this reason, a low growth rate is employed to reduce organic film damage. [11, 12] We anticipated that at a higher growth rate, there would be greater damage due to high energy ITO particle bombardment, while at a lower growth rate, there would be fewer high energy collisions.

We sought to determine whether there was a particular growth rate at which plasma damage was minimized. We predicted that such a rate would be slow enough to minimize plasma exposure, but fast enough to prevent prolonged exposure to elements in the chamber. However, we do not find one particular rate at which damage is mitigated to the greatest extent. Figure 4-11 demonstrates that the facing-target sputter system prevents damage at all growth powers and thus increasing the rate has little effect. Additionally, Figure 4-12 illustrates that the majority of damage occurs at the initial start of plasma sputtering.

Our results show that a facing-target sputter system can maintain relatively low damage even at high growth rates. The difference in PL between the highest and lowest growth rate is approximately 10%, demonstrated in Figure 4-4, whereas in conventional sputter systems, growth rates of ITO sputtered onto organic films are limited to 0.06 Å/s. [10] This is supported by work Hoshi et al., which demonstrates that damage from facing-target sputtering is independent of growth rate. [31] The initial reduction of the PL by 59% for the sample deposited at the slowest rate is likely due to thin film effects associated with a change in the index of refraction mismatch at the air interface. However, plasma induced damage cannot be completely ruled out without applying an optoelectronic model. The excitons generated by the photoexcitation of $Alq_3$ are likely quenched by ITO, suggesting that the presence of ITO would reduce PL. Exciton quenching at the ITO electrode might be expected, yet samples with BPhen of a layer thickness that will suppress quenching show a similar initial drop in PL.

These results suggest that analyzing the various stages of plasma sputtering is key to understanding the mechanisms responsible for film damage.

## 5.3 Distinguishing Damage Mechanisms from PL

There may be five mechanisms, described in Chapter 2, which cause organic film damage during plasma sputtering:

1. ITO atoms
2. High energy ions
3. High energy electrons
4. Secondary electrons
5. Gaseous ions

Analysis of PL for samples with a sputtered ITO film may not allow us to fully assess damage because PL can decrease due to factors separate from organic film damage. One possibility is that the index of refraction is affected by thin-film interference. For this reason, we can not conclusively determine what causes a change in PL. Therefore, we conducted experiments to distinguish between possible mechanisms of damage.

### 5.3.1 Shutter State

#### Shutter Open

Figure 5-1 illustrates the sputter chamber with shutter in the open state. ITO atoms, high energy ions, high energy electrons, secondary electrons, and gaseous ions are exposed to the substrate. While the facing-target is designed to confine high energy ions and electrons within the plasma plume stationed beneath the substrates, some high energy particles may escape and travel beyond the magnetic field to the substrate when the shutter is in the open state.

#### Shutter Closed

While the shutter separating the plasma plume from the substrates, shields hot plasma ions, high energy electrons, and secondary electrons, the suspended gaseous ions may still circumvent the shutter and travel to the substrates. Thus, we can isolate the effect of suspended particles on $Alq_3$ by running the plasma with the shutter in the closed position, illustrated in Figure 5-2.

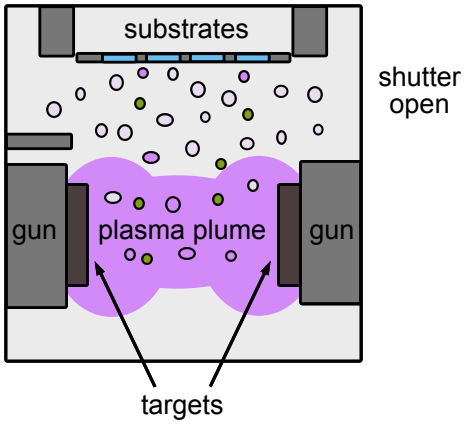



Figure 5-1: Sputter Shutter Open: ITO atoms, high energy ions and electrons, secondary electrons, and gaseous ions can bombard substrates.

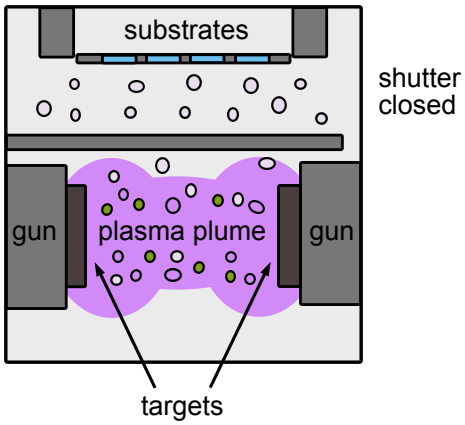



Figure 5-2: Sputter Shutter Closed: High energy ions, electrons, and secondary electrons are confined to plasma plume, ITO atoms are shielded by the shutter, and gaseous ions are located throughout chamber.

### 5.3.2 Plasma Sputtering Stages

Steps involved in depositing an ITO film:

1. Initially, sample sits in the chamber
2. With the shutter closed, gaseous ions are exposed to sample
3. With the shutter open, there is direct exposure to all features of the plasma
4. As ITO is deposited, the ITO film acts as a protection layer, reducing damage with greater thickness

### 5.3.3 Damage by Plasma Sputter Stage

Previous research has demonstrated the harmful nature of gaseous ion irradiation on organic films. [32] We propose that with the shutter closed, gaseous ions may travel through the sputter chamber to damage the substrates. We would expect this to remove the effects of high energy $Ar^+$ ions as well as high energy and secondary electrons. To explore effects aside from the high energy collisions, we performed experiments with the shutter closed, illustrated in Figure 5-2.

We investigated the effect of initial plasma exposure by exposing the bare $Alq_3$ film to elements of the chamber with the shutter closed. Figure 4-3 shows that with a higher growth rate, the PL is reduced, implying greater damage. This suggests that initial exposure of the film to plasma elements in the chamber may dominate $Alq_3$ damage. We attribute this to the absence of an ITO layer which acts as self-protection throughout the growth.

To approximate any measure of self-protection the initial layer of ITO may provide, we employed a BPhen protective layer between $Alq_3$ and ITO. Other studies suggest that a buffer layer may prevent against organic layer damage from both metal deposition by thermal evaporation and ITO deposition by sputtering. [14, 15, 12, 19, 20, 21] Previous work describes the motivation for using BPhen to eliminate exciton quenching at the electrode interface and to protect organic layers from damage when depositing an electrode. [22, 33]

The experiments carried out with the shutter closed allow us to understand the degree of damage that might occur at the onset of sputtering. Figure 4-15 demonstrates that there is greater damage for $Alq_3$ films with no protective layer compared to samples with a BPhen protective layer. For samples with protective BPhen layer, there is a layer protecting $Alq_3$ from incoming ions that result from plasma sputtering.

Figure 4-15 demonstrates that BPhen mitigates damage to $Alq_3$ upon exposure to ozone gas produced during the plasma sputter process. For the samples without a protective layer, gaseous ions may bombard the organic fluorescent layer. However, a protective layer can protect the fluorescent organic layer against gaseous ion bombardment.

Figure 4-15 reveals a trend between growth rate and PL when the shutter is closed. As growth rate is increased, there is greater damage. This demonstrates that initial damage caused by sputtering is dependent on plasma growth rate.

## 5.4 Error and Control Measures

The variation in data presented in Figures 4-3 and 4-7 may be due to sources of experimental error introduced upon fabrication.

The $Alq_3$ and BPhen films were deposited via thermal evaporation. Samples were thermally evaporated at the same time as a control. This allowed us to account for potential differences in the properties of $Alq_3$ and/or BPhen film from different thermal evaporation executions. Immediately following evaporation, the sample was moved to the sputter system. Following plasma sputter operation, the sample was removed and PL was measured for the sample and the control.

Sources of error include possible contamination in the thermal evaporation chamber altering the chemical composition of $Alq_3$ and BPhen. Additionally, variations in the growth rate of the evaporated films could have contributed to different degrees of crystallization of $Alq_3$ or BPhen. All procedures were carried out in a oxygen and moisture controlled Nitrogen glovebox, however, trace amounts of oxygen present in the Argon gas line of the sputter system could have degraded the quality of the $Alq_3$ film.

## 5.5 Summary

Our results suggest that for facing-target magnetron sputtering, ITO growth rate does not significantly affect PL. Our findings show that the majority of organic film damage occurs at the onset of sputtering from exposure to gaseous ions. We also propose that when the shutter is closed, the $Alq_3$ is damaged by exposure to gaseous ions that diffuse throughout the chamber and that this damage depends on growth rate. Lastly, our results suggest that a BPhen protective layer prevents against gaseous ions that could damage a bare $Alq_3$ surface.

# Chapter 6

# Conclusion

This study explored the plasma sputter damage mechanisms of $Alq_3$ through several experiments: (i) in which the shutter was open and an ITO film deposited atop $Alq_3$, (ii) in which the shutter was open and an ITO film deposited on a BPhen layer protecting $Alq_3$, (iii) in which the shutter was closed and $Alq_3$ was exposed to gaseous ions in the plasma sputtering chamber, and (iv) in which the shutter was closed and $Alq_3$ protected with BPhen was exposed to gaseous ions in the plasma sputtering chamber.

We demonstrate that ITO growth rate does not have a significant effect on organic film damage for a facing-target magnetron sputter system. Additionally, our results indicate that organic film damage occurs at the onset of sputtering ITO from exposure to gaseous ions present in the sputtering chamber. We show that a BPhen protective layer can mitigate this damage.

## 6.1 Future work

Future work includes a comparison of substrates sputtered in a facing-target magnetron sputter system with those sputtered in other sputter systems configurations. An alternative approach includes mounting the samples within the plasma plume of the facing-target magnetron sputter system. Placing substrates in the plasma directly, would allow for additional insight into the damage caused by direct plasma exposure. If these substrates vary in PL with respect to the samples deposited with ITO in this study, it would suggest that the facing-target magnetron system properly confines high energy electrons and ions.

While this study considered the effect of growth rate, an additional plasma sputtering parameter which would provide insight on the nature of organic film damage

is chamber pressure. We would expect that organic films would be damaged more severely at higher pressures, where there is a higher concentration of gaseous ions in the chamber.

We can also consider how the optoelectronic properties of the films may affect measured PL. When gaseous Argon ions are exposed to $Alq_3$, the optical properties may be affected by changes to the film morphology. [34, 35] Therefore, optical modeling of ITO, $Alq_3$, and BPhen may help to clarify what changes in PL are due to damage and what changes may be due to variations in the optical properties of the films, such as the index of refraction.

## 6.2 Impacts

Our results suggest that for facing-target magnetron sputter systems, ITO film deposition is not limited to low growth rates in order to prevent organic film damage. This work builds upon previous studies which utilize photoluminecence spectroscopy to study damage caused to organic films during the plasma sputter deposition of ITO. These findings improve our understanding of the damage mechanisms involved in the process of plasma sputtering. This work impacts the application of ITO in organic optoelectronic devices which offer benefits to society, such as organic solar cells.

# Appendix A

# Appendix

## A.1 Fluorescence

Relationship between energy (E), frequency ($\gamma$), and wavelength ($\lambda$), where c is the speed of light and h is Planck's constant:

$$E = h\gamma = \frac{ch}{\lambda} \tag{A.1}$$

## A.2 Photoluminescence (PL) Analysis and Error Propagation Calculations

### A.2.1 Addition of Measured PL

Operation:

$$PL_{sum} = PL_1 + PL_2 + PL_3 \tag{A.2}$$

Error calculation:

$$\delta(PL_{sum}) = \sqrt{(\delta PL_1)^2 + (\delta PL_2)^2 + (\delta PL_3)^2} \tag{A.3}$$

### A.2.2 Average PL

Operation:

$$PL_{average} = \frac{PL_{sum}}{3} \tag{A.4}$$

Error calculation:

$$\delta(PL_{average}) = \mid \frac{1}{3} \mid \cdot(\delta PL_{sum}) \tag{A.5}$$

### A.2.3 Normalized PL

Operation:

$$PL_{normalized} = \frac{PL_{average}}{PL_{control_{maximum}}} \tag{A.6}$$

Error calculation:

$$\delta(PL_{normalized}) = \mid PL_{normalized} \mid \cdot(\delta PL_{average}) \tag{A.7}$$

# Bibliography


[1] Klaus Ellmer. Past achievements and future challenges in the development of optically transparent electrodes. *Nature Photonics*, 6(12):809–817, 2012.

[2] D.S. Ginley and J.D. Perkins. *Handbook of Transparent Conductors*. Springer, 2011.

[3] W.-R. Cao, J. Li, H.Z. Chen, and J.G. Xue. Transparent electrodes for organic optoelectronic devices: a review. *Journal of Photonics for Energy*, 4(1):040990, 2014.

[4] D. Langley, G. Giusti, C. Mayousse, C. Celle, D. Bellet, and J.-P. Simonato. Flexible transparent conductive materials based on silver nanowire networks: a review. *Nanotechnology*, 24(45):452001, 2013.

[5] David S. Hecht, Liangbing Hu, and Glen Irvin. Emerging transparent electrodes based on thin films of carbon nanotubes, graphene, and metallic nanostructures. *Advanced Materials*, 23(13):1482–1513, 2011.

[6] M.N. Gueye, A. Carella, J. Faure-Vincent, R. Demadrille, and J.-P. Simonato. Progress in understanding structure and transport properties of PEDOT-based materials: A critical review. *Progress in Materials Science*, 108:100616, 2020.

[7] Z. Wu. Transparent, conductive carbon nanotube films. *Science*, 305(5688):1273–1276, 2004.

[8] J.S. Moon, J.H. Park, T.Y. Lee, Y.W. Kim, J.B. Yoo, C.Y. Park, J.M. Kim, and K.W. Jin. Transparent conductive film based on carbon nanotubes and PEDOT composites. *Diamond and Related Materials*, 14(11):1882–1887, 2005.

[9] U. Betz, M. Olsson, J. Marthy, M.F. Escola, and F. Atamny. Thin film engineering of indium tin oxide: Large area flat panel displays application. *Surface and Coatings Technology*, 200(20-21):5751–5759, 2006.

[10] V. Bulović, P. Tian, P. E. Burrows, M. R. Gokhale, S. R. Forrest, and M. E. Thompson. A surface-emitting vacuum-deposited organic light emitting device. *Applied Physics Letters*, 70(22):2954–2954, 1997.

[11] H. Lei, K. Ichikawa, Y.-C. Hoshi, M.-H. Wang, T. Uchida, and Y. Sawada. A study of deposition of ITO films on organic layer using facing target sputtering in ar and kr gases. *Thin Solid Films*, 518(11):2926–2929, 2010.

[12] L. S. Liao, L. S. Hung, W. C. Chan, X. M. Ding, T. K. Sham, I. Bello, C. S. Lee, and S. T. Lee. Ion-beam-induced surface damages on tris-(8-hydroxyquinoline) aluminum. *Applied Physics Letters*, 75(11):1619–1621, 1999.

[13] H. Suzuki and M. Hikita. Organic light-emitting diodes with radio frequency sputter-deposited electron injecting electrodes. *Applied Physics Letters*, 68(16):2276–2278, 1996.

[14] H.-K. Kim, D.-G. Kim, K.-S. Lee, M.-S. Huh, S.H. Jeong, K.I. Kim, H. Kim, D.W. Han, and J.H. Kwon. Plasma damage-free deposition of al cathode on organic light-emitting devices by using mirror shape target sputtering. *Applied Physics Letters*, 85(19):4295–4297, 2004.

[15] L.S. Hung, L.S. Liao, C.S. Lee, and S.T. Lee. Sputter deposition of cathodes in organic light emitting diodes. *Journal of Applied Physics*, 86(8):4607–4612, 1999.

[16] M. Matsuoka, Y. Hoshi, and M. Naoe. rf and dc discharge characteristics for opposed-targets sputtering. *Journal of Applied Physics*, 60(6):2096–2102, 1986.

[17] H. Lei, Y. Hoshi, M. Wang, T. Uchida, S. Kobayashi, and S. Yutaka. Electron-bombardment-induced damage to organic light emission layer. *Japanese Journal of Applied Physics*, 49, 2010.

[18] C.-H. Chung, Y.-W. Ko, Y.-H. Kim, C.-Y. Sohn, H.-Y. Chu, S.-H. Ko Park, and J.-H. Lee. Radio frequency magnetron sputter-deposited indium tin oxide for use as a cathode in transparent organic light-emitting diode. *Thin Solid Films*, 491(1):294–297, 2005.

[19] H. Schmidt, H. Flügge, T. Winkler, T. Bülow, T. Riedl, and W. Kowalsky. Efficient semitransparent inverted organic solar cells with indium tin oxide top electrode. *Applied Physics Letters*, 94(24):243302, 2009.

[20] C.-F. Qiu, H.-Y. Chen, Z.-L. Xie, M. Wong, and H.-S. Kwok. 47.2: Hole injection and power efficiency of organic light emitting diodes with ultra-thin inorganic buffer layer on indium tin oxide. *SID Symposium Digest of Technical Papers*, 33(1):1262–1265, 2002.

[21] T. Kim, Y. Firdaus, A. Kirmani, R.-Z. Liang, H.-L. Hu, M.-X. Liu, A. El Labban, S. Hoogland, P.M. Beaujuge, E.H. Sargent, and A. Amassian. Hybrid tandem quantum dot/organic solar cells with enhanced photocurrent and efficiency via ink and interlayer engineering. *ACS Energy Letters*, 3(6):1307–1314, 2018.

[22] Y.-F. Zhao, L. Chen, C. Li, and K. Müllen. Effects of a bathophenanthroline exciton blocking layer on thermal annealing-free bulk heterojunction solar cells. *Synthetic Metals*, 174:46–49, 2013.

[23] S. Weeks. Design of a radio-frequency facing-target sputtering system for low-damage thin film deposition. Senior Thesis, 2013.

[24] H. Lei, M. Wang, Y. Hoshi, T. Uchida, S. Kobayashi, and Y. Sawada. Comparative studies on damages to organic layer during the deposition of ITO films by various sputtering methods. *Applied Surface Science*, 285:389–394, 2013.

[25] Y. Onai, T. Uchida, Y.o Kasahara, K. Ichikawa, and Y. Hoshi. Transparent conductive film for top-emission organic light-emitting devices by low damage facing target sputtering. *Thin Solid Films*, 516(17):5911–5915, 2008.

[26] P.J. Kelly and R.D. Arnell. Magnetron sputtering: a review of recent developments and applications. *Vacuum*, 56(3):159–172, 2000.

[27] Tae Hyun Gil, Christian May, Sebastian Scholz, Sebastian Franke, Michael Toerker, Hubert Lakner, Karl Leo, and Stefan Keller. Origin of damages in OLED from al top electrode deposition by DC magnetron sputtering. *Organic Electronics*, 11(2):322–331, 2010.

[28] Y.-H. Cheng, K.-Y. Lin, Y.-C. Hung, C.-H. Cheng, K.-C. Syao, and M.-C. Lee. Study of ion bombardment effect for $alq_3$ films. *Applied Surface Science*, 252(18):6375–6378, 2006.

[29] A.R. Barron. *Physical Methods in Chemistry and Nano Science*. Addison-Wesley Professional, 2019.

[30] D. T. Harvey. *Modern Analytical Chemistry*. McGraw-Hill, 1999.

[31] Yoichi Hoshi, Hiro-omi Kato, and Kentaro Funatsu. Structure and electrical properties of ITO thin films deposited at high rate by facing target sputtering. *Thin Solid Films*, 445(2):245 – 250, 2003.

[32] L.-S. Hung and J. Madathil. Radiation damage and transmission enhancement in surface-emitting organic light-emitting diodes. *Thin Solid Films*, 410(1):101–106, 2002.

[33] J.G. Jang, H.J. Ji, H.S. Kim, and J.S. Jeong. Tpbi:firpic organic light emitting devices with the electron transport layer of bphen/$alq_3$. *Current Applied Physics*, 11(1, Supplement):S251 – S254, 2011. International Conference on Electronic Materials.

[34] A. Zawadzka, P. Płóciennik, J. Strzelecki, Z. Łukasiak, and B. Sahraoui. Photophysical properties of alq3 thin films. *Optical Materials*, 36(1):91 – 97, 2013. Recent Progress in Advanced Materials for Photonics and Energy Applications.

[35] V.K. Shukla, S. Kumar, and D. Deva. Light induced effects on the morphology and optical properties of tris-(8-hydroxyquinoline) aluminium ($alq_3$) small molecular thin film. *Synthetic Metals*, 156(5):387 – 391, 2006.